Theoretical Evaluation of Offloading through Wireless LANs

Hiroshi Saito and Ryoichi Kawahara
NTT Network Technology Laboratories
3-9-11, Midori-cho, Musashino-shi, Tokyo 180-8585, Japan.
URL: http://www9.plala.or.jp/hslab/
Phone: +81 422 59 4300, Fax: +81 422 59 6364.
saito.hiroshi@lab.ntt.co.jp, kawahara.ryoichi@lab.ntt.co.jp

arXiv:1403.2486v1 [cs.PF] 11 Mar 2014

Abstract

Offloading of cellular traffic through a wireless local area network (WLAN) is theoretically evaluated. First, empirical data sets of the locations of WLAN internet access points are analyzed and an inhomogeneous Poisson process consisting of high, normal, and low density regions is proposed as a spatial point process model for these configurations. Second, performance metrics, such as mean available bandwidth for a user and the number of vertical handovers, are evaluated for the proposed model through geometric analysis. Explicit formulas are derived for the metrics, although they depend on many parameters such as the number of WLAN access points, the shape of each WLAN coverage region, the location of each WLAN access point, the available bandwidth (bps) of the WLAN, and the shape and available bandwidth (bps) of each subregion identified by the channel quality indicator in a cell of the cellular network. Explicit formulas strongly suggest that the bandwidth a user experiences does not depend on the user mobility. This is because the bandwidth available by a user who does not move and that available by a user who moves are the same or approximately the same as a probabilistic distribution. Numerical examples show that parameters, such as the size of regions where placement of WLAN access points is not allowed and the mean density of WLANs in high density regions, have a large impact on performance metrics. In particular, a homogeneous Poisson process model as the WLAN access point location model largely overestimates the mean available bandwidth for a user and the number of vertical handovers. The overestimated mean available bandwidth is, for example, about 50% in a certain condition.

Keywords: Offload, performance evaluation, spatial characterization of network, access point configuration, spatial point process, inhomogeneous Poisson process, integral geometry (geometric probability), cellular network (mobile network), wireless LAN, internet access, handover (handoff), coverage.

I. Introduction

Due to the surge in data traffic, cellular network operators need to make large investments in their networks. For example, AT&T acknowledged a 50-fold growth in wireless data traffic in a 3-year period, and KT, the largest network operator in Korea, experienced a 10-fold data traffic increase in its wideband code-division multiple access (WCDMA) network [1]. Although these operators invested extensively in their cellular networks, further efforts are necessary. The provision of wireless local area network (WLAN) access points (APs) is expected to be one of the most promising ways of mitigating the surge in traffic in cellular networks [2],[3]. In addition to the deployment of WLAN APs by cellular network operators, independent operators also provide these points in order to offer Internet access services and obtain subscriber fees from users. Generally, WLAN internet access services are cheaper and faster than Internet access through cellular networks, although their coverage regions are limited. Thus, vertical handover (handoff) can occur at the boundary of the WLAN coverage region between the WLAN and cellular network.

Although the relationship between cellular networks and public WLAN services is important, quantitative analysis of this relationship is, as far as we know, very limited. Choi et al. [1] compared the traffic growth of KT's WCDMA, WiMAX, and WLAN networks in 2010 and included some quantitative information. However, they describe the situation only from a macroscopic point of view and do not include any information for each WLAN AP (microscopic point of view) or any theoretical work.

This paper examines a theoretical evaluation of the offloading of cellular networks through public WLAN services and consists of two parts. The first part uses empirical data on the locations of public WLAN internet APs and analyzes them as a spatial point process. An inhomogeneous Poisson process is proposed as a model of the configurations of public WLAN Internet APs. Based on the proposed model, the second part analyzes the performance metrics for the inhomogeneous Poisson process model through integral geometry and derives the formulas for the performance metrics.

Much progress has been made in spatial characterization techniques over the past few decades, and these techniques have been applied in many fields including epidemiological analysis, earthquake occurrence analysis, natural resource distribution, geological analysis, agricultural production, and biological analysis [4], [5], [6], [7]. However, research related to the first part, that is, spatial characterization of networks including APs and base station placement, has not been sufficiently investigated. Riihijärvi et al. investigated spatial characterization of wireless systems [8], [9], [10]. They analyzed the spatial structure of

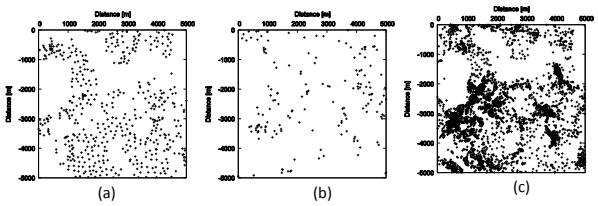

Fig. 1. Locations of public WLAN access points

WLAN AP locations on the east and west coasts of the USA [8]. They found that measured AP locations feature power-law or scale-free behavior in their correlation structures. They analyzed WLAN AP location data and insisted that the Geyer saturation model as a spatial point process fits the actual data [9]. Michalopoulou et al. [10] quantified the dependence between the node distributions of wireless networks (second and third generation (2G/3G) cellular networks) and the underlying population densities. They showed significant statistical similarities between the locations of 2G base stations and population since the deployment of 2G base stations is complete. In addition, Andrews et al. [11] compared the coverage based on the placement of actual base stations and those derived by the Poisson point process. However, the main focus of this study is the derivation of the signal-to-interference-and-noise ratio and information on the actual base station locations or modeling for them is lacking. Even when we consider wired access networks, we can see that spatial characterization models have not been extensively studied. Gloaguen et al. [12], [13] focused on the fact that the actual configuration of the wired subscriber network strongly depends on the physical route of roads and derives its stochastic model based on the road configuration model. Their results enable us to remove time-consuming tasks, such as inputting road data or other geographical information, when we conduct simulations for network evaluation.

Integral geometry (geometric probability) used in the second part of this paper is a mathematical method for evaluating the measures in which a certain set (normally a subset of a plane) satisfies certain characteristics and has been included in several papers regarding network related issues. For example, a series of papers [14], [15], [16] based on analysis using integral geometry proposed shape estimation methods for a target object based on reports from sensor nodes whose locations are unknown. Lazos et al. [17] and Lazos and Poovendran [18] directly applied the results of the integral geometry discussed in Chapter 5 Section 6.7 of [19] in an analysis of detecting an object moving in a straight line and in evaluating the probability of k-coverage. Kwon and Shroff [20] also applied integral geometry in an analysis of straight line routing, which is an approximation of shortest path routing, and Choi and Das [21] used it to select sensors in energy-conserving data gathering. Currently, integral geometry is also being applied to network survivability studies [22], [23].

This paper is organized as follows. In Section 2, empirical data sets of locations of public WLAN Internet APs are analyzed. Section 3 provides basic formulas used in the analysis in the following sections. A model proposed based on the results of Section 2 is described in Section 4. Sections 5 and 6 evaluate performance metrics before and after introducing WLANs, respectively. Numerical examples are given in Section 7, and a conclusion is given in Section 8.

II. Empirical data analysis

We used the location data of public WLAN APs of three operators (a), (b), (c) in Tokyo (Fig. 1). (These data were obtained on April 20th, 2012 [24], October 7th, 2011 [25], and October 20th, 2011 [26].) Figure 1 shows three graphs, which respectively correspond to the three individual operators. The upper left corners of the graphs represent Shinjuku, one of the busiest regions in Tokyo. We used the location data in this 5×5 km square region.

In the remainder of this section, we investigate the spatial point process model for the AP locations. First, we investigate the hypothesis that they follow a homogeneous Poisson process. Because the statistics using empirical data reject the hypothesis and show that they are more clustered, we also investigate a model that is more clustered than a homogeneous Poisson process. Although there are many possible spatial point processes, we propose to adopt an inhomogeneous Poisson process for the model because the number of APs deployed by individual operators at each subregion show high cross-correlations.

A. Test of homogeneous Poisson process

We conducted a significance test of the null hypothesis of a homogeneous Poisson process. We divided the entire region into subregions and counted the number of APs in each region. Let $a_i(j)$ be the number of APs provided by the j-th operator in the i-th subregion, A_j be the sample mean of the number of APs provided by the j-th operator ($A_j \stackrel{\text{def}}{=} \sum_{i=1}^{n_a} a_i(j)/n_a$), and V_j be its sample variance($V_j \stackrel{\text{def}}{=} \sum_{i=1}^{n_a}(a_i(j) - A_j))^2/(n_a - 1)$), where n_a is the number of subregions. The index of dispersion $I_d(j)$ proposed by Sachs was applied to the WLAN APs deployed by the j-th operator: $I_d(j) \stackrel{\text{def}}{=} (n_a - 1)V_j/A_j$ (p.54 in [6]). For a significance test of the null hypothesis of a homogeneous Poisson process, $I_d(j)$ follows a χ^2 distribution with the $n_a - 1$ degree of freedom ([6], p.104 in [5]). The index I_d for each operator and two-side 5% bounds of χ^2 for

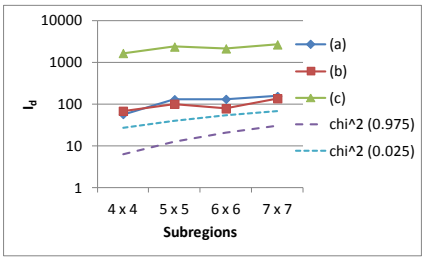

Fig. 2. Test using I_d.

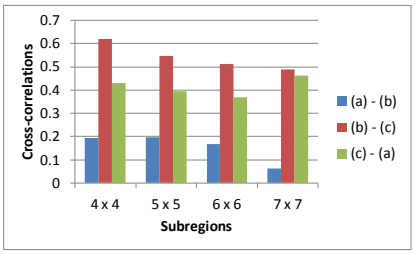

Fig. 3. Cross correlations of $\{a_i(j)\}_i$ and $\{a_i(k)\}_i$

the hypothesis of a homogeneous Poisson process are plotted in Fig. 2. The results in Fig. 2 indicate that we can reject the hypothesis of a homogeneous Poisson process of significance level 0.05. That is, $\{\mathbf{w}_i\}_i$ is more clustered than a homogeneous Poisson process, where $\mathbf{w}_i$ is the location of the i-th WLAN AP.

B. Inhomogeneous Poisson process

By carefully observing the maps in Fig. 1, we can see that all three operators have some common sparse regions. These are regions such as parks or shrines; therefore, WLAN APs are not allowed or it is practically impossible to place them in these regions. We should adopt a model that can describe this fact. Similarly, the operators also have busy regions in common, for example, regions around train/subway stations. To evaluate whether there are common sparse/busy regions, the cross-correlations $c(j,k)$ of $\{a_i(j)\}_i$ and $\{a_i(k)\}_i$ were evaluated, where $c(j,k)$ is defined as follows: $c(j,k) \stackrel{\text{def}}{=} \frac{\sum_i (a_i(j)-A_j)(a_i(k)-A_k)}{(n_a-1)\sqrt{V_j V_k}}$. Figure 3 shows that there are non-negligible cross correlations, particularly between (b) and (c) and between (c) and (a).

Spatial point process models can be classified into two types. In the first type, the placement of WLAN APs is assumed to be mainly determined by the locations of other WLAN APs. We call these internal models. Typical examples of internal models are Matern, simple sequential inhibition, and Gibbs point processes [4],[6]. In the other type, which we call external models, the placement of APs is assumed to be mainly determined by the location features of the APs themselves, rather than the locations of other APs. An inhomogeneous Poisson process, i.e., a Poisson process with inhomogeneous intensity, is a typical example of an external model. Because an inhomogeneous Poisson process model is one in which each point location is determined independently of the other point locations (unlike the other typical models described above), we adopt an inhomogeneous Poisson process as a spatial point process model for $\{\mathbf{w}_i\}_i$. In practice, it is impossible for us to reject the internal model based on the data that we have. However, because of this cross-correlation analysis and the fact that the high- or low-density subregions are closely related to the existence of facilities there, we assume the approximation that the WLAN AP locations follow an inhomogeneous Poisson process with intensity $\lambda(\mathbf{x})$, where $\lambda(\mathbf{x})$ is the function of location $\mathbf{x}$.

Assuming that $\{\mathbf{w}_i\}_i$ follow an inhomogeneous Poisson process, the later sections analyze, derive, and evaluate performance metrics, such as mean available bandwidth for a user and the number of vertical handovers through integral geometry.

III. Preliminaries for Analysis

A. Notation

In the remainder of this paper, $\|X\|$ denotes the size of X, $|X|$ denotes the perimeter length of X, ∂X denotes the boundary of X, and $\overline{X}$ denotes the complementary set (region) of X for region $X \subset \mathbb{R}^2$. In addition, for a given line G, $\sigma(X)$ denotes the length of the chord $X \cap G$. For regions $X, Y \subset \mathbb{R}^2$, $l_{\partial X \cap Y}$ denotes the length of the arc created by ∂X and Y, that is, the part of ∂X included in Y.

B. Integral geometry and geometric probability

We introduce the concepts of integral geometry and geometric probability [19] as a preliminary to the following analysis.

Consider a bounded set $X \subset \mathbb{R}^2$ and a condition X_c. A typical example of X_c is $X_c = \{X \cap X_1 \neq \emptyset\}$ for a given set X_1. Here, X is, for example, a region covered by a WLAN AP and X_1 is the cell of a cellular network. Integral geometry provides a method for measuring the expectation of the quantity $q(X)$ for the set of positions of X satisfying a condition X_c. Then, if we would like to consider the size of the intersection of X and X_1 when X intesects X_1, set $q(X) = \|X \cap X_1\|$ and $X_c = \{X \cap X_1 \neq \emptyset\}$.

For a set of X whose position is defined by the reference point (x, y) and the angle θ that a reference line fixed in X makes with another reference line fixed to the fixed coordinates, integral geometry defines $E[q(X)]$ by $\int_{X_c} q(X)dX / \int_{X_c} dX = \int_{X_c} q(X)dx\,dy\,d\theta / \int_{X_c} dx\,dy\,d\theta$. The numerator means the integral of $q(X)$ at a position (x, y, θ) uniformly over the possible parameter space (x, y, θ) satisfying X_c, and the denominator means the area size of the parameter space (x, y, θ) satisfying X_c. That is, the numerator is (roughly speaking) a summation of $q(X)$ at every points specified by (x, y, θ) satisfying X_c, and the denominator is (roughly speaking) the number of points satisfying X_c. Therefore, it is an expectation of $q(X)$.

In particular, if $q(X) = \mathbf{1}$ (the position (x, y, θ) satisfies Y_c) where $\mathbf{1}(\cdot)$ denotes the indicator function and $Y_c \subseteqq X_c$, $E[q(X)] = \int_{Y_c} dx\,dy\,d\theta / \int_{X_c} dx\,dy\,d\theta = \Pr(Y_c|X_c)$ is the (conditional) probability of the positions of X satisfying a condition Y_c among the positions of X satisfying a condition X_c. (This is called a geometric probability [19].) In this sense, $\int_{Y_c} dx\,dy\,d\theta$ is a non-normalized probability, because it is proportional to the probability and normalized by $\int_{X_c} dx\,dy\,d\theta$. In the remainder of this paper, this non-normalized probability is called the measure of the set of positions of X satisfying a condition Y_c.

A simple example is shown in Fig. 4, where X is a disk of radius r_x, $X_c = \{X \cap X_1 \neq \emptyset\}$, X_1 is a disk of radius r_{x1}, $Y_c = \{X \cap X_2 \neq \emptyset\}$, and $X_2 \subset X_1$ is a disk of radius r_{x2}. Because this example is independent of θ, we can easily draw a picture. Because integral geometry implicitly assumes that the position (x, y, θ) uniformly moves in the parameter space (if not explicitly indicated otherwise), we can easily understand that $\Pr(Y_c|X_c)$ is given by $\int_{Y_c} dx\,dy\,d\theta / \int_{X_c} dx\,dy\,d\theta = \int_{Y_c} dx\,dy / \int_{X_c} dx\,dy = (r_{x2} + r_x)^2/(r_{x1} + r_x)^2$.

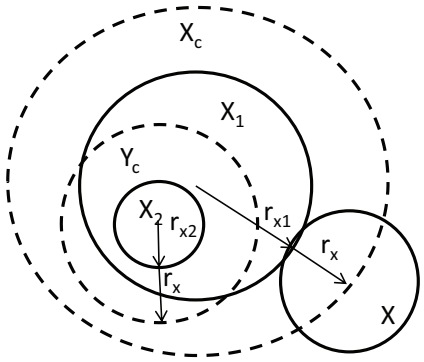

Fig. 4. Simple example

When X is a line G, we should use the parameterization by the angle θ, in which the direction perpendicular to G is a fixed direction ($-\pi \leq \theta \leq \pi$), and by its distance p from the origin O ($0 \leq p$). (We can use another parameterization, but we cannot calculate the integral uniformly over the possible parameter space X_c when the parameters θ and p are not used. This is because integral geometry requires the calculated results to be invariant under the group of motions in the plane.) By using θ and p, the expectation of the quantity $q(G)$ satisfying X_c can be calculated by $\int_{X_c} q(G)dG / \int_{X_c} dG = \int_{X_c} q(G)dp\,d\theta / \int_{X_c} dp\,d\theta$.

In Section VI-B, we assume that a user moves on G. By defining X_c such that G intersects the cell and setting $q(G)$ as the chord length of G in the cell, we can calculate the mean distance (that is, the mean length of the chord) that a user moves in the cell.

C. Known basic formulas

The following basic formulas are known or directly derived through integral geometry.

Accoring to Eqs. (3.12) and (3.6) in [19], for a fixed convex set K, the measure in which the set of positions of a line G that meets K is given by

$$\int_{K \cap G \neq \emptyset} dG = |K|, \tag{1}$$

and the (non-normalized) mean length of the chord made by ∂K and G is given by

$$\int_{K \cap G \neq \emptyset} \sigma(K) dG = \pi \|K\|. \tag{2}$$

For a fixed convex set K_0, the measure of the set of positions of a convex set K_1 that meets K_0 is given as follows (Eq. (6.48) in [19]).

$$\int_{K_0 \cap K_1 \neq \emptyset} dK_1 \quad = \quad f(K_0, K_1) \tag{3}$$

where $f(X,Y) \stackrel{\rm def}{=} 2\pi(\|X\| + \|Y\|) + |X| \cdot |Y|$.

Particularly when K_0 is a point, Eq. (3) becomes

$$\int_{K_0 \cap K_1 \neq \emptyset} dK_1 = 2\pi \|K_1\|. \tag{4}$$

For a fixed convex set K_0, the measure of the set of positions of a convex set K_1 that is contained in K_0 is given as follows (Eq. (6.52) in [19]).

$$\int_{K_1 \subset K_0} dK_1 \quad = \quad 2\pi(\|K_0\| + \|K_1\|) - |K_0| \cdot |K_1| \tag{5}$$

Formally speaking, additional conditions on the curvature of ∂K_0 and that of ∂K_1 are needed for Eq. (5) where ∂K for a set $K \subset \mathbb{R}^2$ means the boundary of K.

For a fixed set K_0, the integral of $\|K_0 \cap K_1\|$ over the position of the set of K_1 is given as follows. (Eq. (6) is Eq. (6.57) in [19]. Although Eq. (6.57) in [19] does not include π, Eqs. (6.55) and (6.56) used in [19] to derive Eq. (6.57) show that Eq. (6) is correct and the original Eq. (6.57) in [19] is incorrect.).

$$\int_{K_0 \cap K_1 \neq \emptyset} \|K_0 \cap K_1\| dK_1 \quad = \quad 2\pi \|K_0\| \cdot \|K_1\| \tag{6}$$

Due to Eq. (6.61) in [19] and Eq. (5), Eq. (7) concerning the integral of $l_{\partial K_1 \cap K_0}$ (the length of the arc of ∂K_1 intersecting K_0) is given as follows.

$$\begin{aligned} \int_{\partial K_0 \cap K_1 \neq \emptyset} l_{\partial K_1 \cap K_0} dK_1 \quad &= \quad \int_{K_0 \cap K_1 \neq \emptyset} l_{\partial K_1 \cap K_0} dK_1 - \int_{K_1 \subset K_0} |K_1| dK_1 \\ &= \quad 2\pi \|K_0\| \cdot |K_1| - |K_1|(2\pi(\|K_0\| + \|K_1\|) - |K_0| \cdot |K_1|) \\ &= \quad |K_1|(|K_0| \cdot |K_1| - 2\pi \|K_1\|) \end{aligned} \tag{7}$$

Based on Eq. (6), for any $K_2 \subset K_0$,

$$\int_{K_0 \cap K_1 \neq \emptyset} \|K_2 \cap K_1\| dK_1 = \int_{K_2 \cap K_1 \neq \emptyset} \|K_2 \cap K_1\| dK_1 = 2\pi \|K_1\| \cdot \|K_2\| \tag{8}$$

This is because (i) $\int_{K_0 \cap K_1 \neq \emptyset} \|K_2 \cap K_1\| dK_1 = \int_{K_2 \cap K_1 \neq \emptyset} \|K_2 \cap K_1\| dK_1 + \int_{K_2 \cap K_1 = \emptyset, K_0 \cap K_1 \neq \emptyset} \|K_2 \cap K_1\| dK_1$, and (ii) the second term is 0 due to $\|K_2 \cap K_1\| = 0$ for $K_2 \cap K_1 = \emptyset$.

D. Extension of basic formulas

To analyze an inhomogeneous Poisson process, we propose the following extensions for the basic formulas mentioned above. We assume that Ω is a convex set and that $dK_1 = d\mathbf{w}\ d\gamma$ where $\mathbf{w}$ is a reference point in K_1, and γ is the angle characterizing K_1. These extensions require that the reference point $\mathbf{w}$ must be within Ω. For a fixed K_0, the relative location of Ω is assumed to be fixed. In the following, the term $\hat{r}(K_1)$ is similar to the radius of K_1, and we adopt the definition $\hat{r}(K_1) \stackrel{\rm def}{=} |K_1|/(2\pi)$. This term is identical to the radius when K_1 is a disk.

Eqs. (3) and (5) are approximately extended to the following. For a fixed convex set K_0, the measure of the set of positions of a convex set K_1 that meets K_0 and is contained in K_0 are given as follows.

$$\int_{K_0 \cap K_1 \neq \emptyset, \mathbf{w} \in \Omega} d\mathbf{w}\ d\gamma \quad \approx \quad 2\pi(\|K_0 \cap \Omega\| + \hat{r}(K_1) l_{\partial K_0 \cap \Omega}) \tag{9}$$

$$\int_{K_1 \subset K_0, \mathbf{w} \in \Omega} d\mathbf{w}\ d\gamma \quad \approx \quad 2\pi(\|K_0 \cap \Omega\| - \hat{r}(K_1) l_{\partial K_0 \cap \Omega}) \tag{10}$$

This is due to Fig. 5-(a), (b) where the gray regions indicate where $\mathbf{w}$ can exist. Thus, the right-hand sides of Eqs. (9) and (10) are approximations of the size of these regions times 2π.

When K_0 is a point, the following approximation, which is an analogy of Eq. (4), is proposed.

$$\int_{K_0 \cap K_1 \neq \emptyset, \mathbf{w} \in \Omega} d\mathbf{w}\ d\gamma \quad \approx \quad 2\pi \|K_1\| \Pr(K_0 \in \Omega) \tag{11}$$

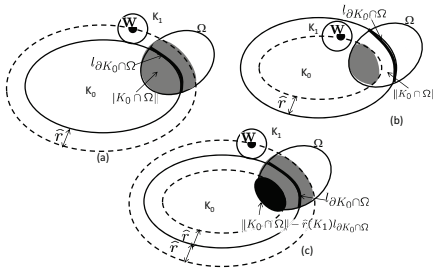

Fig. 5. Derivations of approximations

Eq. (6) is approximately extended to the following. For a fixed set K_0, the integral of $\|K_0 \cap K_1\|$ and the integral of $l_{\partial K_1 \cap K_0}$ over positions of a set K_1 are given as follows.

$$\begin{aligned}\int_{K_0 \cap K_1 \neq \emptyset, \mathbf{w} \in \Omega} \|K_0 \cap K_1\| d\mathbf{w}\ d\gamma &\approx 2\pi\{(\|K_0 \cap \Omega\| - \hat{r}(K_1) l_{\partial K_0 \in \Omega})\|K_1\| + 2\hat{r}(K_1) l_{\partial K_0 \in \Omega}(\|K_1\|/2)\} \\ &= 2\pi \|K_1\| \cdot \|K_0 \cap \Omega\| \end{aligned} \tag{12}$$

This is due to Fig. 5-(c). Here, $\|K_0 \cap K_1\|$ becomes $\|K_1\|$ for $\mathbf{w}$ in the black region in this figure, and it becomes approximately half of $\|K_1\|$ for $\mathbf{w}$ in the gray region. The size of the black region is approximately $\|K_0 \cap \Omega\| - \hat{r}(K_1) l_{\partial K_0 \in \Omega}$ and that of the gray region is approximately $2\hat{r}(K_1) l_{\partial K_0 \in \Omega}$. Therefore, we obtain Eq. (12).

Applying Eq. (12), for any $K_2 \subset K_0$,

$$\int\limits_{K_0 \cap K_1 \neq \emptyset, \mathbf{w} \in \Omega} \|K_2 \cap K_1\| d\mathbf{w}\ d\gamma = \int_{K_2 \cap K_1 \neq \emptyset, \mathbf{w} \in \Omega} \|K_2 \cap K_1\| d\mathbf{w}\ d\gamma \approx 2\pi \|K_1\| \cdot \|K_2 \cap \Omega\| \tag{13}$$

Eq. (7) is approximately extended to the following. Because $l_{\partial K_1 \cap K_0} \approx |K_1|/2$ and $\int_{\partial K_0 \cap K_1 \neq \emptyset, \mathbf{w} \in \Omega} d\mathbf{w} \approx 2\hat{r}(K_1) l_{\partial K_0 \cap \Omega}$,

$$\int\limits_{\partial K_0 \cap K_1 \neq \emptyset, \mathbf{w} \in \Omega} l_{\partial K_1 \cap K_0} d\mathbf{w}\ d\gamma \approx 2\pi \hat{r}(K_1) l_{\partial K_0 \cap \Omega} |K_1|. \tag{14}$$

Eqs. (9), (10), (12) (as a result, Eq. (13)), and (14) are exact when ∂K_0 is a line segment in Ω, K_1 is a disk with radius r_{K_1}, and $\partial\Omega \subset (\overline{K_0} \cap (K_0 \oplus r_{K_1}))$ is a line segment vertical to ∂K_0 where $K_0 \oplus r_{K_1}$ is a Minkoski sum of K_0 and a disk with radius r_{K_1}.

IV. Model

We focus on a single cell of a cellular network and WLAN APs around it for the remainder of this paper. The subregion of this cell can be classified according to the radio channel quality, which identifies the channel quality indicator (CQI) [27], [28], [29]. Let C_i be a region in the cell where the CQI is i. Let us assume that $C_n \subset C_{n-1} \subset \cdots \subset C_1 = C$ and that $C_{n+1} = \emptyset$ to simplify the notation. Let s_i be the achieved bitrate (bps) of the radio channel used in $C_i - C_{i+1}$.

Suppose that a public WLAN is provided to offload Internet access traffic. The i-th WLAN AP is located at $\mathbf{w}_i$ and has the coverage region D_i with the angle γ_i made by a reference line fixed in D_i and a reference line fixed to the fixed coordinates where $C \cap D_i \neq \emptyset$ $(1 \leq i \leq l)$. In the remainder of this paper, we use the following assumptions if not explicitly indicated otherwise:

- C_i and D_j are convex;
- The set of locations $\{\mathbf{w}_i\}_i$ indepedently follows an inhomogeneous Poisson process with intensity $\lambda(\mathbf{x})$ at $\mathbf{x}$;
- $\lambda(\mathbf{x}) = \begin{cases} \lambda_H, & \text{for } \mathbf{x} \in \text{high density region } \Omega_H \subset \mathbb{R}^2, \\ \lambda_L, & \text{for } \mathbf{x} \in \text{low density region } \Omega_L \subset \mathbb{R}^2, \\ \lambda_0, & \text{for } \mathbf{x} \notin \Omega_H, \Omega_L \end{cases}$ where $\lambda_L \leq \lambda_0 \leq \lambda_H$;
- $\Omega_H \cap \Omega_L = \emptyset$;
- γ_i is uniformly distributed;
- When a user can use either a cellular network or WLAN, he/she uses the WLAN;
- The relative locations of Ω_H and Ω_L from C are fixed;
- Locations of line G are indepepndent of $\{\mathbf{w}_i\}_i$.

Let s_w be the available bandwidth (bps) of the WLAN, the relative additional intensity $\rho_H \stackrel{\text{def}}{=} (\lambda_H - \lambda_0)/\lambda_0$, the relative reduced intensity $\rho_L \stackrel{\text{def}}{=} (\lambda_0 - \lambda_L)/\lambda_0$, the mean intensity $\lambda_C \stackrel{\text{def}}{=} \{\lambda_H \|C \cap \Omega_H\| + \lambda_L \|C \cap \Omega_L\| + \lambda_0(\|C\| - \|C \cap \Omega_H\| - \|C \cap \Omega_L\|)\}/\|C\|$, and the relative normal region intensity $\rho_0 \stackrel{\text{def}}{=} \lambda_0/\lambda_C$.

This paper addresses the mean number N_h of vertical handovers between the cell and a WLAN coverage region and the two types of mean available bandwidth and probability in which a user can use the bandwidth (bps) faster than a certain value as performance metrics. The first type of mean available bandwidth is called the static available bandwidth B_s (bps), i.e., the bandwidth available by a user who does not move, and the second type is the dynamic available bandwidth, B_d (bps), i.e., the bandwidth available by a user who moves. B_s and B_d are the main performance metrics from the user point of view. On the other hand, N_h is important mainly from a network operator point of view because additional tasks are required in the network at the handover. For metric x, $\tilde{x}$ denotes x without introducing a public WLAN.

The mean total throughput T_d is defined by the sum of bits that a user moving on a line G ($C \cap G \neq \emptyset$) at a unit speed in the cell can send by making full use of the radio channel if no other competing users, and it is averaged over various positions of G. B_s is the mean available bandwidth at which users distributed uniformly over C can use the radio channel if no other competing users, and B_d is the ratio of the mean total throughput T_d to the mean total sojourn time within the cell. The total sojourn time is defined by the sum of times during which a user moving on a line G ($C \cap G \neq \emptyset$) at a unit speed stays in the cell and it is averaged over various positions of G. In addition, let $q_s(x)$ ($q_d(x)$) be the probability that a user staying somewhere in C (moving on a line G at a unit speed) can use the bandwidth (bps) faster than x.

Throughout the analysis, the times for signaling and its processing, the influence of other competing users, and the interference between WLAN APs are not considered. Therefore, this analysis provides ideal performance.

V. Theoretical analysis without introducing WLANs

This section derives the performance metrics when WLANs are not introduced.

Because the probability that a point randomly chosen in C is in $C_i - C_{i+1}$ is $(\|C_i\| - \|C_{i+1}\|)/\|C\|$, we obtain the following result.

Result 1: The mean and cumulative probabilistic distribution of the bandwidth available by the user who does not move are given as follows.

$$\tilde{B}_s = \frac{\sum_{i=1}^{n}(\|C_i\| - \|C_{i+1}\|)s_i}{\|C\|} \tag{15}$$

$$\tilde{q}_s(x) = \frac{\sum_{i=1}^{n}(\|C_i\| - \|C_{i+1}\|)\mathbf{1}(s_i \geq x)}{\|C\|} \tag{16}$$

Consider a line $G(\theta, p)$. Assume that a tagged user moves on $G(p, \theta)$ at a unit speed.

Result 2:

$$\tilde{B}_d \stackrel{\text{def}}{=} \frac{\tilde{T}_d}{\int_{C\cap G\neq\emptyset}\sigma(C)dG/\int_{C\cap G\neq\emptyset}dG} = \tilde{B}_s, \tag{17}$$

$$\tilde{q}_d(x) \stackrel{\text{def}}{=} \frac{\int_{C\cap G\neq\emptyset}\sum_{i=1}^{n}\sigma(C_i - C_{i+1})\mathbf{1}(s_i \geq x)dG}{\int_{C\cap G\neq\emptyset}\sigma(C)dG} = \tilde{q}_s(x), \tag{18}$$

$$\tilde{N}_h = 0. \tag{19}$$

Here, the mean total throughput $\tilde{T}_d$ is given as follows: $\tilde{T}_d \stackrel{\text{def}}{=} \frac{\int_{C\cap G\neq\emptyset}\sum_{i=1}^{n} s_i\sigma(C_i - C_{i+1})dG}{\int_{C\cap G\neq\emptyset}dG} = \sum_{i=1}^{n}\pi(\|C_i\| - \|C_{i+1}\|)s_i/|C|$.

Proof: The length $\sigma(C_i - C_{i+1})$ of the chord $G(p, \theta) \cap (C_i - C_{i+1})$ is given by the following equation due to Eq. (2), for $1 \leq i \leq n$.

$$\int_{C\cap G\neq\emptyset}\sigma(C_i - C_{i+1})dG = \int_{C_i\cap G\neq\emptyset}\sigma(C_i)dG - \int_{C_{i+1}\cap G\neq\emptyset}\sigma(C_{i+1})dG = \pi(\|C_i\| - \|C_{i+1}\|) \tag{20}$$

Because we consider the set of lines $\{C \cap G \neq \emptyset\}$, we need to normalize by $\int_{C\cap G\neq\emptyset}dG$. Therefore, using Eq. (1), we obtain $\tilde{T}_d$.

Because the mean length of the chord $G \cap C$ is $\int_{C\cap G\neq\emptyset}\sigma(C)dG/\int_{C\cap G\neq\emptyset}dG = \pi\|C\|/|C|$, we obtain Eqs. (17) and (18). Because there are no WLANs, $\tilde{N}_h = 0$. □

VI. Theoretical analysis after introducing WLANs

This section derives the performance metrics when WLANs are introduced. Because it seems impossible to derive explicit formulas for the performance metrics under an inhomogeneous Poisson process, they are approximation formulas. However, they become exact under a homogeneous Poisson process.

In the remaining, we use the notation $C_x \cap_{i=i_1,\cdots,i_m} D_i \stackrel{\text{def}}{=} C_x \cap D_{i_1} \cap D_{i_2} \cap \cdots \cap D_{i_m}$, $\{C_x \cap D_i \neq \emptyset\}_{i=1}^{l} \stackrel{\text{def}}{=} \{C_x \cap D_1 \neq \emptyset, \cdots, C_x \cap D_l \neq \emptyset\}$, and $(dD)^l \stackrel{\text{def}}{=} dD_1 \ \cdots \ dD_l$. Here, C_x is C or C_i, $(i = 1, \cdots, l)$.

At the beginning, we provide the following result, which is often used in the remaining in this section.

Result 3: Under a homogeneous Poisson process,

$$\int_{\{C\cap D_i\neq\emptyset\}_{i=1}^{l}} (dD)^l = \Pi_{i=1}^{l} f(C, D_i). \tag{21}$$

Under an inhomogeneous Poisson process,

$$\int_{\{C\cap D_i\neq\emptyset\}_{i=1}^{l}} (dD)^l \approx \rho_0^l \Pi_{i=1}^{l} g_1(C, D_i) \tag{22}$$

where $g_1(C, D_i) \stackrel{\rm def}{=} f(C, D_i) + 2\pi(\rho_H(\|C \cap \Omega_H\| + \hat{r}(D_i) l_{\partial C\cap\Omega_H}) - \rho_L(\|C \cap \Omega_L\| + \hat{r}(D_i) l_{\partial C\cap\Omega_L}))$.

Proof: Under a homogeneous Poisson process, by repeatedly applying Eq. (3), we obain Eq. (21).

For an inhomogeneous Poisson process, λ_H (λ_L, λ_0) is the intensity that a WLAN internet AP is located in the high (low, normal) density region. Therefore, for an arbitrary functon ϕ and any condition X_c,

$$\lambda_C \int_{X_c} \phi \, dD_i = \lambda_0 \int_{X_c, \mathbf{w}_i \in \overline{\Omega_H \cup \Omega_L}} \phi \, d\mathbf{w}_i \; d\gamma_i + \lambda_H \int_{X_c, \mathbf{w}_i \in \Omega_H} \phi \, d\mathbf{w}_i \; d\gamma_i + \lambda_L \int_{X_c, \mathbf{w}_i \in \Omega_L} \phi \, d\mathbf{w}_i \; d\gamma_i.$$

As a result,

$$\int_{X_c} \phi \, dD_i = \rho_0 \{ \int_{X_c, \mathbf{w}_i \in \mathbb{R}^2} \phi \, d\mathbf{w}_i \; d\gamma_i + \rho_H \int_{X_c, \mathbf{w}_i \in \Omega_H} \phi \, d\mathbf{w}_i \; d\gamma_i - \rho_L \int_{X_c, \mathbf{w}_i \in \Omega_L} \phi \, d\mathbf{w}_i \; d\gamma_i \}. \tag{23}$$

Set $X_c = C \cap D_i \neq \emptyset$ and $\phi = 1$, and apply Eq. (23). Because of Eqs. (3) and (9),

$$\begin{aligned} \int_{C\cap D_i\neq\emptyset} dD_i &= \rho_0 \{ \int_{C\cap D_i\neq\emptyset, \mathbf{w}_i \in \mathbb{R}^2} d\mathbf{w}_i \; d\gamma_i + \rho_H \int_{C\cap D_i\neq\emptyset, \mathbf{w}_i \in \Omega_H} d\mathbf{w}_i \; d\gamma_i - \rho_L \int_{C\cap D_i\neq\emptyset, \mathbf{w}_i \in \Omega_L} d\mathbf{w}_i \; d\gamma_i \} \\ &\approx \rho_0 g_1(C, D_i). \end{aligned} \tag{24}$$

□

A. Derivation of B_s and $q_s(x)$

This subsection provides B_s and $q_s(x)$. First, we evaluate the expected area size of $C_j \cap_{m=i_1,\cdots,i_k} D_m$ under the condition $\{C \cap D_i \neq \emptyset\}_{i=1}^{l}$. Second, by describing p_j, which is the probability that the point is in $C_j - C_{j+1}$ and is covered by at least a single WLAN, with this expected area size, we derive p_j. Third, based on p_j, B_s and $q_s(x)$ are derived.

1) Derivation of $E[\|C_j \cap_{m=i_1,\cdots,i_k} D_m\| \; |\{C \cap D_i \neq \emptyset\}_{i=1}^{l}]$: Let $E[\|C_j \cap_{m=i_1,\cdots,i_k} D_m\| \; |\{C \cap D_i \neq \emptyset\}_{i=1}^{l}]$ be the expected area size of $C_j \cap_{m=i_1,\cdots,i_k} D_m$ under the condition $\{C \cap D_i \neq \emptyset\}_{i=1}^{l}$.

This expected area size is given by the following.

Result 4:

$$E[\|C_j \cap_{m=i_1,\cdots,i_k} D_m\| \; |\{C \cap D_i \neq \emptyset\}_{i=1}^{l}] \stackrel{\rm def}{=} \frac{\int_{\{C\cap D_i\neq\emptyset\}_{i=1}^{l}} \|C_j \cap_{m=i_1,\cdots,i_k} D_m\| (dD)^l}{\int_{\{C\cap D_i\neq\emptyset\}_{i=1}^{l}} (dD)^l} \tag{25}$$

The denominator is given by Eq. (21) or (22). The numerator is given by Eq. (26) or (27) shown below.

For a homogeneous Poisson process

$$\begin{aligned} &\int_{\{C\cap D_i\neq\emptyset\}_{i=1}^{l}} \|C_j \cap_{m=i_1,\cdots,i_k} D_m\| (dD)^l \\ =\; &\|C_j\| \Pi_{i\neq i_1,\cdots,i_k} f(C, D_i) \cdot \Pi_{j=i_1,\cdots,i_k} (2\pi \|D_j\|). \end{aligned} \tag{26}$$

For an inhomogeneous Poisson process,

$$\begin{aligned} &\int_{\{C\cap D_i\neq\emptyset\}_{i=1}^{l}} \|C_j \cap_{m=i_1,\cdots,i_k} D_m\| (dD)^l \\ \approx\; &\rho_0^l g_2(C_j, k) \Pi_{i\neq i_1,\cdots,i_k} g_1(C, D_i) \cdot \Pi_{m=i_1,\cdots,i_k} (2\pi \|D_m\|) \end{aligned} \tag{27}$$

where $g_2(C_j, k) \stackrel{\rm def}{=} \|C_j\| + \|C_j \cap \Omega_H\|((1+\rho_H)^k - 1) + \|C_j \cap \Omega_L\|((1-\rho_L)^k - 1)$.

Proof: For a homogeneous Poisson process, repeatedly apply Eqs. (3) and (8) to obtain Eq. (26).

$$\begin{aligned} &\int_{\{C\cap D_i\neq\emptyset\}_{i=1}^{l}} \|C_j \cap_{m=i_1,\cdots,i_k} D_m\| (dD)^l \\ =\; &\Pi_{i\neq i_1,\cdots,i_k} f(C, D_i) \int_{C\cap D_{i_1}\neq\emptyset,\cdots,C\cap D_{i_k}\neq\emptyset} \|C_j \cap_{m=i_1,\cdots,i_k} D_m\| dD_{i_1} \cdots dD_{i_k} \\ =\; &(2\pi\|D_{i_k}\|) \Pi_{i\neq i_1,\cdots,i_k} f(C, D_i) \int_{C\cap D_{i_1}\neq\emptyset,\cdots,C\cap D_{i_{k-1}}\neq\emptyset} \|C_j \cap_{m=i_1,\cdots,i_{k-1}} D_m\| dD_{i_1} \cdots dD_{i_{k-1}} \\ =\; &\|C_j\| \Pi_{i\neq i_1,\cdots,i_k} f(C, D_i) \cdot \Pi_{j=i_1,\cdots,i_k} (2\pi \|D_j\|). \end{aligned}$$

The proof for an inhomogeneous Poisson process is in Appendix A.□

2) Derivation of p_j: In this subsection, we derive the probability that a randomly chosen point is in $C_j - C_{j+1}$ and is covered by at least a single WLAN. By using this probability, the performance metrics are derived later.

For a randomly chosen point $\mathbf{x} \in C$, let p_j be the probability that the point is in $C_j - C_{j+1}$ and is covered by at least a single WLAN. According to the definition of a geometric probability,

$$\begin{aligned} p_j &\stackrel{\text{def}}{=} \Pr(\mathbf{x} \in C_j - C_{j+1}, \mathbf{x} \in \bigcup_{i=1}^{l} D_i, D_i \cap C \neq \emptyset, i = 1, \cdots, l | \mathbf{x} \in C, D_i \cap C \neq \emptyset, i = 1, \cdots, l) \\ &= \frac{\int_{\mathbf{x} \in C_j - C_{j+1}, \mathbf{x} \in \bigcup_{i=1}^{l} D_i, \{C \cap D_i \neq \emptyset\}_{i=1}^{l}} d\mathbf{x}\ (dD)^l}{\int_{\mathbf{x} \in C, \{C \cap D_i \neq \emptyset\}_{i=1}^{l}} d\mathbf{x}\ (dD)^l}. \end{aligned} \tag{28}$$

By using $E[\|C_j \cap_{m=i_1,\cdots,i_k} D_m\|\ |\{C \cap D_i \neq \emptyset\}_{i=1}^{l}]$, we can describe p_j.

Result 5:

$$\begin{aligned} p_j &= \frac{1}{\|C\|} \sum_{m=1}^{l} \sum_{1 \leq i_1 < \cdots < i_m \leq l} (-1)^{m-1} (E[\|C_j \cap_{i=i_1,\cdots,i_m} D_i\|\ |\{C \cap D_i \neq \emptyset\}_{i=1}^{l}] \\ &\qquad - E[\|C_{j+1} \cap_{i=i_1,\cdots,i_m} D_i\|\ |\{C \cap D_i \neq \emptyset\}_{i=1}^{l}]). \end{aligned} \tag{29}$$

Proof: Due to Eq. (4),

$$p_j = \frac{\int_{\{C \cap D_i \neq \emptyset\}_{i=1}^{l}} \|(C_j - C_{j+1}) \cap (\bigcup_{i=1}^{l} D_i)\| (dD)^l}{\|C\| \int_{\{C \cap D_i \neq \emptyset\}_{i=1}^{l}} (dD)^l}. \tag{30}$$

Apply the following equations to the numerator.

$$\|(C_j - C_{j+1}) \cap (\bigcup_{i=1}^{l} D_i)\| = \|\bigcup_{i=1}^{l} (C_j \cap D_i)\| - \|\bigcup_{i=1}^{l} (C_{j+1} \cap D_i)\| \tag{31}$$

$$\|\bigcup_{i=1}^{l} (C_j \cap D_i)\| = \sum_{i=1}^{l} \|C_j \cap D_i\| - \sum_{1 \leq i_1 < i_2 \leq l} \|C_j \cap D_{i_1} \cap D_{i_2}\| + \cdots, \tag{32}$$

$$\begin{aligned} &\int_{\{C \cap D_i \neq \emptyset\}_{i=1}^{l}} \|(C_j - C_{j+1}) \cap (\bigcup_{i=1}^{l} D_i)\| (dD)^l \\ &= \int_{\{C \cap D_i \neq \emptyset\}_{i=1}^{l}} \sum_{m=1}^{l} \sum_{1 \leq i_1 < \cdots < i_m \leq l} (-1)^{m-1} \|C_j \cap_{i=i_1,\cdots,i_m} D_i\| - \|C_{j+1} \cap_{i=i_1,\cdots,i_m} D_i\| (dD)^l. \end{aligned} \tag{33}$$

Apply the definition by Eq.(25) to the equation above, we obtain Eq. (29). □

Eq. (29) is intuitive. Because the point $\mathbf{x}$ is randmly chosen, p_j is proportional to the area size of $(C_j - C_{j+1}) \cap (\bigcup_{i=1}^{l} D_i)$. By taking into account the overlaps, we obtain Eq. (33), which is essentially the same with Eq. (29).

We are now in the postion to describe p_j.

Result 6: Under an inhomogeneous Poisson process, p_j is approximately given by

$$p_j \approx \frac{\sum_{m=1}^{l} (-1)^{m-1} (g_2(C_j, m) - g_2(C_{j+1}, m)) b_h(m|C)}{\|C\|} \tag{34}$$

where $b_h(m|C) \stackrel{\text{def}}{=} \sum_{1 \leq i_1 < \cdots < i_m \leq l} \Pi_{i=i_1,\cdots,i_m} (2\pi \|D_i\| / g_1(C, D_i))$.

For $j = 1, \cdots, n$, when $\|D_i\| = \|D\|$ and $|D_i| = |D|$ for all i, Eq. (34) becomes

$$p_j \approx \frac{(1 - b_0) g_0(j) + (1 - b_H) g_H(j) + (1 - b_L) g_L(j)}{\|C\|} \tag{35}$$

where $g_H(j) \stackrel{\text{def}}{=} \|C_j \cap \Omega_H\| - \|C_{j+1} \cap \Omega_H\|$, $g_L(j) \stackrel{\text{def}}{=} \|C_j \cap \Omega_L\| - \|C_{j+1} \cap \Omega_L\|$, $g_0(j) \stackrel{\text{def}}{=} \|C_j - C_{j+1}\| - g_H(j) - g_L(j)$, $b_0 \stackrel{\text{def}}{=} (1 - \frac{2\pi \|D\|}{g_1(C,D)})^l$, $b_H \stackrel{\text{def}}{=} (1 - \frac{2\pi(1+\rho_H)\|D\|}{g_1(C,D)})^l$ and $b_L \stackrel{\text{def}}{=} (1 - \frac{2\pi(1-\rho_L)\|D\|}{g_1(C,D)})^l$.

Under a homegneous Poisson process, this approximation formula becomes exact and simplified into

$$p_j = \frac{\|C_j - C_{j+1}\|}{\|C\|} \{1 - \Pi_{i=1}^{l} (1 - \frac{2\pi \|D_i\|}{f(C, D_i)})\}. \tag{36}$$

Proof of Eq. (34):

Apply Eqs. (22) and (27) to Eq. (25).

$$\begin{aligned} & E[\|C_j \cap_{m=i_1,\cdots,i_k} D_m\| \ |\{C \cap D_i \neq \emptyset\}_{i=1}^{l}] \\ \approx \ & g_2(C_j,k)\Pi_{m=i_1,\cdots,i_k}(2\pi\|D_m\|/g_1(C,D_m)) \end{aligned} \tag{37}$$

According to Eq. (29),

$$\begin{aligned} p_j &\approx \frac{1}{\|C\|}\sum_{m=1}^{l}\sum_{1\le i_1<\cdots<i_m\le l}(-1)^{m-1}(g_2(C_j,m)-g_2(C_{j+1},m))\Pi_{k=i_1,\cdots,i_m}(2\pi\|D_k\|/g_1(C,D_k)) \\ &= \frac{1}{\|C\|}\sum_{m=1}^{l}(-1)^{m-1}(g_2(C_j,m)-g_2(C_{j+1},m))b_h(m|C). \end{aligned} \tag{38}$$

□

Proof of Eq. (35): Note $b_h(m|C) = {}_lC_m(2\pi\|D\|/g_1(C,D))^m$ and $g_2(C_j,m)-g_2(C_{j+1},m) = g_0(j)+(1+\rho_H)^m g_H(j)+(1-\rho_L)^m g_L(j)$. Because $\sum_{m=1}^{l}(-1)^{m-1}{}_lC_m(2\pi\|D\|/g_1(C,D))^m = 1-(1-2\pi\|D\|/g_1(C,D))^l$, $\sum_{m=1}^{l}(-1)^{m-1}{}_lC_m(2\pi\|D\|(1+\rho_H)/g_1(C,D))^m = 1-(1-2\pi\|D\|(1+\rho_H)/g_1(C,D))^l$, and $\sum_{m=1}^{l}(-1)^{m-1}{}_lC_m(2\pi\|D\|(1-\rho_L)/g_1(C,D))^m = 1-(1-2\pi\|D\|(1-\rho_L)/g_1(C,D))^l$, Eq. (35) is derived. □

Proof of Eq. (36): For a homogeneous Poisson process, apply Eqs. (25), (21), and (26) to Eq. (29).

$$\begin{aligned} p_j &= \frac{1}{\|C\|}\sum_{m=1}^{l}\sum_{1\le i_1<\cdots<i_m\le l}(-1)^{m-1}(\|C_j\|-\|C_{j+1}\|)\Pi_{j=i_1,\cdots,i_m}(2\pi\|D_j\|/f(C,D_i)) \\ &= \frac{\|C_j\|-\|C_{j+1}\|}{\|C\|}\{1-\Pi_{i=1}^{l}(1-\frac{2\pi\|D_i\|}{f(C,D_i)})\}. \end{aligned} \tag{39}$$

□

Under a homogeneous Poisson process, $\Omega_H = \Omega_L = \emptyset$ and $\rho_H = \rho_L = 0$. Thus, $g_1(C,D_i) = f(C,D_i)$ and $g_2(C_j,k) = \|C_j\|$. Then, p_j given by Eq. (34) becomes identical to that given by Eq. (36). That is, the approximation formula Eq. (34) is exact under a homogeneous Poisson process.

The meaning of Eq. (36) is as follows. Because the probability that a point $\mathbf{x}$ in C is covered by D_i when $C \cap D_i \neq \emptyset$ is $\frac{\int_{\mathbf{x}\cap D_i\neq\emptyset} dD_i}{\int_{C\cap D_i\neq\emptyset} dD_i} = \frac{2\pi\|D_i\|}{f(C,D_i)}$ due to Eqs. (3) and (4), $\{1-\Pi_{i=1}^{l}(1-\frac{2\pi\|D_i\|}{f(C,D_i)})\}$ indicates the probability that a point in C will be covered by at least one of $D_1,\cdots,D_l$ when they are independently deployed. Of course, $\frac{\|C_j-C_{j+1}\|}{\|C\|}$ is the probability that a point in C is in $C_j - C_{j+1}$.

Similarly, we can consider the meaning of Eq. (34). When $\rho_0 = 1$, $b_h(m|C)$ is approximately the probability that a point in C is covered by m of $D_1,\cdots,D_l$ because $\frac{2\pi\|D_i\|}{g_1(C,D_i)}$ is approximately the probability that a point in C is covered by D_i intersecting C. In addition, $g_2(C_j,m)$ is the size of C_j modified by the clustered effect because of C_j intersecting m of $D_1,\cdots,D_l$. Thus, $(g_2(C_j,m)-g_2(C_{j+1},m))b_h(m|C)/\|C\|$ is approximately the probability that a point in C is in $C_j - C_{j+1}$ and covered by m of $D_1,\cdots,D_l$ intersecting C. The event in which a point is covered by at least a single WLAN is identical to the occurrence of events in which a point is covered by an individual WLAN. However, these events are not exclusive. Therefore, the term $\sum_{m=1}^{l}(-1)^{m-1}$ taking account of the overlaps of these events appears.

3) Derivation of B_s and $q_s(x)$ based on p_j: By using the result mentioned above, we can derive B_s and $q_s(x)$.

Result 7: Under an inhomogeneous Poisson process, B_s and $q_s(x)$ (the mean and the cumulative probabilisitic distribution of the available bandwidth that the user who does not move) are approximately given by

$$B_s \approx \sum_{j=1}^{n}[\frac{\|C_j\|-\|C_{j+1}\|}{\|C\|}s_j + \frac{s_w-s_j}{\|C\|}\sum_{m=1}^{l}(-1)^{m-1}(g_2(C_j,m)-g_2(C_{j+1},m))b_h(m|C)], \tag{40}$$

$$\begin{aligned} q_s(x) \approx \ & \sum_{j=1}^{n}[\frac{\|C_j\|-\|C_{j+1}\|}{\|C\|}\mathbf{1}(s_j \ge x) \\ & + \frac{\mathbf{1}(s_w \ge x)-\mathbf{1}(s_j \ge x)}{\|C\|}\sum_{m=1}^{l}(-1)^{m-1}(g_2(C_j,m)-g_2(C_{j+1},m))b_h(m|C)]. \end{aligned} \tag{41}$$

Under a homogeneous Poisson process, these approximation formulas become exact and simplified into

$$B_s = s_w - \sum_{j=1}^{n}\frac{(s_w-s_j)\|C_j-C_{j+1}\|}{\|C\|}\Pi_{i=1}^{l}(1-\frac{2\pi\|D_i\|}{f(C,D_i)}) \tag{42}$$

$$q_s(x) = \sum_{j=1}^{n}\frac{\|C_j\|-\|C_{j+1}\|}{\|C\|}[\mathbf{1}(s_w \ge x)\{1-\Pi_{i=1}^{l}(1-\frac{2\pi\|D_i\|}{f(C,D_i)})\} + \mathbf{1}(s_j \ge x)\Pi_{i=1}^{l}(1-\frac{2\pi\|D_i\|}{f(C,D_i)})]. \tag{43}$$

Proof: Because the probability that the point $\mathbf{x}$ is in $C_j - C_{j+1}$ but is not covered by any WLANs is $\frac{\|C_i - C_{i+1}\|}{\|C\|} - p_j$,

$$B_s = \sum_{j=1}^{n}(p_j s_w + (\frac{\|C_j\| - \|C_{j+1}\|}{\|C\|} - p_j)s_j), \tag{44}$$

$$q_s(x) = \sum_{j=1}^{n}(p_j \mathbf{1}(s_w \geq x) + (\frac{\|C_j\| - \|C_{j+1}\|}{\|C\|} - p_j)\mathbf{1}(s_j \geq x)). \tag{45}$$

Under a homogeneous Poisson process, because p_j is given by Eq. (36), B_s and $q_s(x)$ are given by Eqs. (42) and (43).
Under an inhomogeneous Poisson process, due to Eq. (34), B_s and $q_s(x)$ are given by Eqs. (40) and (41).
□

In Eq. (40), the first term $\frac{\|C_j\| - \|C_{j+1}\|}{\|C\|} s_j$ means that the bit rate s_j is available with the probability that a point in C is located in $C_j - C_{j+1}$, and the second term means that the additional bit rate $s_w - s_j$ is available with probability p_j. Eq. (42) means that a WLAN bit rate s_w is available but the bit rate may be reduced to s_j with the probability that a point in C is included in $C_j - C_{j+1}$ and not covered by any WLANs.

Similarly to Eq. (35), Eqs. (40) and (41) can be simplfied when $\|D_i\| = \|D\|$ and $|D_i| = |D|$ for all i.

B. Derivation of B_d and $q_d(x)$

For each G, define $\sigma_w \stackrel{\text{def}}{=} \sigma(C \cap \bigcup_{i=1}^{l} D_i)$ and $\sigma_i \stackrel{\text{def}}{=} \sigma((C_i - C_{i+1}) \cap \overline{\bigcup_{j=1}^{l} D_j})$. Here, σ_w (σ_i) is a part of G where a user moving on G can use the WLAN (the cellular network with achieved bitrate s_i).

This subsection evaluates the mean dynamic available bandwidth B_d and its cumulative probabilistic distribution $q_d(x)$ defined below.

$$B_d \stackrel{\text{def}}{=} T_d \frac{\int_{C\cap G\neq\emptyset} dG}{\int_{C\cap G\neq\emptyset} \sigma(C) dG} = \frac{T_d|C|}{\pi\|C\|} \tag{46}$$

$$q_d(x) \stackrel{\text{def}}{=} \frac{\int_{C\cap G\neq\emptyset, \{C\cap D_i\neq\emptyset\}_{i=1}^{l}} (\mathbf{1}(s_w \geq x)\sigma_w + \sum_{i=1}^{n} \mathbf{1}(s_i \geq x)\sigma_i) dG\ (dD)^l}{\int_{C\cap G\neq\emptyset, \{C\cap D_i\neq\emptyset\}_{i=1}^{l}} \sigma(C) dG\ (dD)^l} \tag{47}$$

Here, the mean total throughput T_d is defined by $T_d \stackrel{\text{def}}{=} \frac{\int_{C\cap G\neq\emptyset, \{C\cap D_i\neq\emptyset\}_{i=1}^{l}} (s_w\sigma_w + \sum_{i=1}^{n} s_i\sigma_i) dG\ (dD)^l}{\int_{C\cap G\neq\emptyset, \{C\cap D_i\neq\emptyset\}_{i=1}^{l}} dG\ (dD)^l}$.

First, the expected length of σ_w and that of σ_i are described by $E[\|C_j \cap_{m=i_1,\cdots,i_k} D_m\| \ |\{C \cap D_i \neq \emptyset\}_{i=1}^{l}]$. Second, the mean total throughput T_d is derived based on them. Third, B_d and $q_d(x)$ are derived based on T_d.

1) Describing the expected chord length with the condition $C \cap G \neq \emptyset, \{C \cap D_i \neq \emptyset\}_{i=1}^{l}$: The expected σ_w and σ_i with the condition $C \cap G \neq \emptyset, \{C \cap D_i \neq \emptyset\}_{i=1}^{l}$ are defined as follows.

$$E[\sigma_x | C \cap G \neq \emptyset, \{C \cap D_i \neq \emptyset\}_{i=1}^{l}] \stackrel{\text{def}}{=} \frac{\int_{C\cap G\neq\emptyset, \{C\cap D_i\neq\emptyset\}_{i=1}^{l}} \sigma_x dG\ (dD)^l}{\int_{C\cap G\neq\emptyset, \{C\cap D_i\neq\emptyset\}_{i=1}^{l}} dG\ (dD)^l} \tag{48}$$

where $\sigma_x = \sigma_w$ or σ_i. To my surprise, the conditional expectations of σ_w and σ_i can be described by the conditional expectation of $\|C_j \cap_{m=i_1,\cdots,i_k} D_m\|$.

Result 8:

$$E[\underset{l}{\sigma_w} | C \cap G \neq \emptyset, \{C \cap D_i \neq \emptyset\}_{i=1}^{l}] = \pi \sum_{m=1}^{l} (-1)^{m-1} \sum_{1\leq i_1<\cdots<i_m\leq l} E[\|C \cap_{k=i_1,\cdots,i_m} D_k\| \ |\{C \cap D_i \neq \emptyset\}_{i=1}^{l}]/|C|, \tag{49}$$

$$E[\underset{l}{\sigma_i} | C \cap G \neq \emptyset, \{C \cap D_i \neq \emptyset\}_{i=1}^{l}] = \pi \sum_{m=0}^{l} (-1)^{m} \sum_{1\leq i_1<\cdots<i_m\leq l} E[\|C_i \cap_{k=i_1,\cdots,i_m} D_k\| - \|C_{i+1} \cap_{k=i_1,\cdots,i_m} D_k\| \ |\{C \cap D_j \neq \emptyset\}_{j=1}^{l}]/|C|. \tag{50}$$

Proof of Eq. (49): According to the definition of σ_w,

$$\int_{C\cap G\neq\emptyset} \sigma_w dG = \int_{C\cap G\neq\emptyset} \{\sum_{i=1}^{l} \sigma(C \cap D_i) - \sum_{1\leq i_1<i_2\leq l} \sigma(C \cap D_{i_1} \cap D_{i_2}) + \cdots\} dG. \tag{51}$$

Note that $C \cap D_{i_1} \cap D_{i_2} \cap \cdots$ is convex. Hence, by using Eq. (2), we obtain

$$\int_{C\cap G\neq\emptyset} \sigma(C \cap_{i=i_1,i_2,\cdots} D_i) dG$$

$$= \int_{C\cap D_{i_1}\cap D_{i_2}\cap\cdots\cap G\neq\emptyset} \sigma(C\cap_{i=i_1,i_2,\ldots} D_i)dp\,d\theta$$
$$= \pi\|C\cap_{i=i_1,i_2,\ldots} D_i\|. \quad (52)$$

Thus,

$$\int_{C\cap G\neq\emptyset,\{C\cap D_i\neq\emptyset\}_{i=1}^l} \sigma_w dG\ (dD)^l$$
$$= \pi\int_{\{C\cap D_i\neq\emptyset\}_{i=1}^l} \{\sum_{i=1}^l \|C\cap D_i\| - \sum_{1\leq i_1<i_2\leq l}\|C\cap D_{i_1}\cap D_{i_2}\| + \cdots\}\ (dD)^l. \quad (53)$$

On the other hand, the denominator of Eq. (48) is $|C|\int_{\{C\cap D_i\neq\emptyset\}_{i=1}^l}(dD)^l$ because of Eq. (1). Due to Eq. (25), we obtain Eq.(49). □

Proof of Eq. (50):

$$\int_{C\cap G\neq\emptyset}\sigma_i dG = \int_{C\cap G\neq\emptyset}\{\sigma(C_i\cap\overline{\bigcup_{j=1}^l D_j}) - \sigma(C_{i+1}\cap\overline{\bigcup_{j=1}^l D_j})\}dG$$
$$= \int_{C\cap G\neq\emptyset}\{\sigma(C_i) - \sigma(C_i\cap\bigcup_{j=1}^l D_j) - \sigma(C_{i+1}) + \sigma(C_{i+1}\cap\bigcup_{j=1}^l D_j)\}dG$$
$$= \int_{C\cap G\neq\emptyset}\{\sigma(C_i) - \sigma(\bigcup_{j=1}^l (C_i\cap D_j)) - \sigma(C_{i+1}) + \sigma(\bigcup_{j=1}^l (C_{i+1}\cap D_j))\}dG. \quad (54)$$

Because of the definition of $\sigma(\bigcup_{j=1}^l (C_i\cap D_j))$,

$$\int_{C\cap G\neq\emptyset}\sigma(\bigcup_{j=1}^l (C_i\cap D_j))dG = \int_{C\cap G\neq\emptyset}\{\sum_{j=1}^l \sigma(C_i\cap D_j) - \sum_{1\leq j_1<j_2\leq l}\sigma(C_i\cap D_{j_1}\cap D_{j_2}) + \cdots\}dG. \quad (55)$$

Note that $C_i\cap D_{j_1}\cap D_{j_2}\cap\cdots$ is convex. Due to a similar equation to Eq. (52), we obtain the following equation.

$$\int_{C\cap G\neq\emptyset,\{C\cap D_i\neq\emptyset\}_{i=1}^l}\sigma_i dG\ (dD)^l$$
$$= \pi\int_{\{C\cap D_i\neq\emptyset\}_{i=1}^l}\{\|C_i\| - \sum_{j=1}^l\|C_i\cap D_j\| + \sum_{1\leq j_1<j_2\leq l}\|C_i\cap D_{j_1}\cap D_{j_2}\| - \cdots$$
$$-\|C_{i+1}\| + \sum_{j=1}^l\|C_{i+1}\cap D_j\| - \sum_{1\leq j_1<j_2\leq l}\|C_{i+1}\cap D_{j_1}\cap D_{j_2}\| + \cdots\}(dD)^l. \quad (56)$$

Because the denominator of Eq. (48) is $|C|\int_{\{C\cap D_i\neq\emptyset\}_{i=1}^l}(dD)^l$ and because of Eq. (25), we obtain Eq. (50). □

2) Derivation of T_d: Note that $T_d = E[s_w\sigma_w + \sum_{i=1}^n s_i\sigma_i | C\cap G\neq\emptyset, \{C\cap D_j\neq\emptyset\}_{j=1}^l]$. Because of Eqs. (49) and (50),

$$T_d = \frac{\pi}{|C|}\sum_{m=0}^l(-1)^{m+1}\sum_{1\leq i_1<\cdots<i_m\leq l}$$
$$E[s_w\|C\cap_{k=i_1,\cdots,i_m} D_k\|\mathbf{1}(m>0) - \sum_{i=1}^n s_i(\|C_i\cap_{k=i_1,\cdots,i_m} D_k\| - \|C_{i+1}\cap_{k=i_1,\cdots,i_m} D_k\|)\ |\{C\cap D_j\neq\emptyset\}_{j=1}^l] \quad (57)$$

By replacing C_j with C in Result 4 (that is, Eqs. (21), (22), (26), and (27)), $E[\|C\cap_{k=i_1,\cdots,i_m} D_k\|\ |\{C\cap D_j\neq\emptyset\}_{j=1}^l] = \|C\|\Pi_{k=i_1,\cdots,i_m}(2\pi\|D_k\|/f(C,D_k))$ for a homogeneous Poisson process and $E[\|C\cap_{k=i_1,\cdots,i_m} D_k\|\ |\{C\cap D_j\neq\emptyset\}_{j=1}^l] \approx g_2(C,m)\Pi_{k=i_1,\cdots,i_m}(2\pi\|D_k\|/g_1(C,D_k))$ for an inhomogeneous Poisson process. In addition, by using Eqs. (21) and (26) for a homogeneous Poisson process and by using Eqs. (27) and (22), we obtain the following result.

Result 9: For an inhomogeneous Poisson process,

$$T_d \approx \frac{\pi}{|C|}\sum_{m=0}^l(-1)^{m+1}\{s_w g_2(C,m)\mathbf{1}(m>0) - \sum_{i=1}^n s_i(g_2(C_i,m) - g_2(C_{i+1},m))\}b_h(m|C), \quad (58)$$

and for a homogeneous Poisson process,

$$T_d = \frac{\pi}{|C|}\{s_w\|C\|(1-\prod_{k=1}^l(1-2\pi\|D_k\|/f(C,D_k))) + \sum_{i=1}^n s_i(\|C_i\| - \|C_{i+1}\|)\prod_{k=1}^l(1-2\pi\|D_k\|/f(C,D_k))\}. \quad (59)$$

3) Derivation of B_d from T_d and $q_d(x)$: Now we are in a position to obtain B_d and $q_d(x)$.

Result 10: Under an inhomogeneous Poisson process, B_d and $q_d(x)$ are approximately given by

$$B_d \approx \sum_{m=0}^{l}(-1)^{m+1}\{s_w g_2(C,m)\mathbf{1}(m>0) - \sum_{i=1}^{n} s_i(g_2(C_i,m) - g_2(C_{i+1},m))\}b_h(m|C)/\|C\| \tag{60}$$

$$q_d(x) \approx \frac{1}{\|C\|}\sum_{m=0}^{l}(-1)^{m+1}\{\mathbf{1}(s_w \geq x, m>0)g_2(C,m) - \sum_{i=1}^{n}\mathbf{1}(s_i \geq x)(g_2(C_i,m) - g_2(C_{i+1},m))\}b_h(m|C). \tag{61}$$

Under a homogeneous Poisson process, these approximation formulas become exact and simplified into

$$B_d = s_w - \sum_{i=1}^{n}(s_w - s_i)\frac{\|C_i\| - \|C_{i+1}\|}{\|C\|}\Pi_{j=1}^{l}(1 - \frac{2\pi\|D_j\|}{f(C,D_j)}). \tag{62}$$

$$q_d(x) = \sum_{j=1}^{n}\frac{\|C_j\| - \|C_{j+1}\|}{\|C\|}[\mathbf{1}(s_w \geq x)\{1 - \Pi_{i=1}^{l}(1 - \frac{2\pi\|D_i\|}{f(C,D_i)})\} + \mathbf{1}(s_j \geq x)\Pi_{i=1}^{l}(1 - \frac{2\pi\|D_i\|}{f(C,D_i)})]. \tag{63}$$

Proof: Because $B_{=}T_d|C|/(\pi\|C\|)$, Eq. (60) is derived directly from Eq. (58). In addition, because of $\|C\| = \sum_{j=1}^{n}\|C_j\| - \|C_{j+1}\|$, Eq. (62) is derived from Eq. (59).

Because of the definition of $q_d(x)$ given by Eq. (47),

$$q_d(x) = \frac{\int_{C\cap G\neq\emptyset,\{C\cap D_i\neq\emptyset\}_{i=1}^{l}} dG\ (dD)^l}{\int_{C\cap G\neq\emptyset,\{C\cap D_i\neq\emptyset\}_{i=1}^{l}} \sigma(C)dG\ (dD)^l}E[\mathbf{1}(s_w \geq x)\sigma_w + \sum_{i=1}^{n}\mathbf{1}(s_i \geq x)\sigma_i | C\cap G\neq\emptyset, \{C\cap D_i\neq\emptyset\}_{i=1}^{l}]. \tag{64}$$

We can evaluate $E[\mathbf{1}(s_w \geq x)\sigma_w + \sum_{i=1}^{n}\mathbf{1}(s_i \geq x)\sigma_i | C\cap G\neq\emptyset, \{C\cap D_i\neq\emptyset\}_{i=1}^{l}]$ by replacing s_w with $\mathbf{1}(s_w \geq x)$ and s_i with $\mathbf{1}(s_i \geq x)$ in derivation of Eqs. (58) and (59). Because $\frac{\int_{C\cap G\neq\emptyset,\{C\cap D_i\neq\emptyset\}_{i=1}^{l}} dG\ (dD)^l}{\int_{C\cap G\neq\emptyset,\{C\cap D_i\neq\emptyset\}_{i=1}^{l}} \sigma(C)dG\ (dD)^l} = |C|/(\pi\|C\|)$, we obtain Eq. (61) and (63). □

Under a homogeneous Poisson process, Eqs. (60) and (61) are identical to Eqs. (62) and (63), respectively. That is, the approximation formulas Eqs. (60) and (61) become exact under a homogeneous Poisson process.

Due to Eqs. (42), (43), (62), and (63),

Result 11: $B_s = B_d$ and $q_s(x) = q_d(x)$ under a homogeneous Poisson process.

In addition, we can see that Eqs. (40), (41) are identical to Eqs. (60) and (61) when $\|D_i\| = \|D\|$ and $|D_i| = |D|$ for all i. That is, the approximation formulas for B_s ($q_s(x)$) are also applicable as those for B_d ($q_d(x)$) when $\|D_i\| = \|D\|$ and $|D_i| = |D|$, even under an inhomogeneous Poisson process.

Therefore, it is strongly suggested that the bit rate a user experiences does not depend on user mobility.

C. Derivation of N_h

Vertical handovers are handovers between a cellular network and a WLAN, and occur when a user moves from one network to the other network. Generally, vertical handovers occur at the boundary of C or that of D_i ($i = 1, 2, \cdots$). We focus on the vertical handovers at the boundary of D_i within C occurring when a user moving along G passes through the boundary of D_i from outside D_i into D_i within C or from inside D_i to outside D_i within C if the passing point $\partial D_i \cap G$ is not covered by any other WLANs.

To evaluate N_h, we define L_h and A_h. When $D_i \cap \partial C \neq \emptyset$, we can define L_h as a line segment between two end points of $D_i \cap \partial C$ and A_h as a convex region surrounded by L_h and $D_i \cap \partial C$ in D_i (Fig. 6).

Let S_i be the number of intersections between G and ∂D_i, $E[S_i|\mathrm{E1}]$ be its expectation when $D_i \subset C, C\cap G\neq\emptyset$, and $E[S_i|\mathrm{E2}]$ be its expectation when $D_i \cap \partial C \neq \emptyset, C\cap G\neq\emptyset$. Because $C\cap G\neq\emptyset$ is satisfied when $G\cap D_i\neq\emptyset, D_i\subset C$ or when $G\cap L_h\neq\emptyset$,

$$E[S_i|\mathrm{E1}] = 2\Pr(G\cap D_i\neq\emptyset, D_i\subset C) = \frac{2\int_{D_i\subset C, D_i\cap G\neq\emptyset} dG\, dD_i}{\int_{C\cap G\neq\emptyset, C\cap D_i\neq\emptyset} dG\ dD_i}, \tag{65}$$

According to Eq. (1) and because of $A_h \subset D_i \cap C$,

$$E[S_i|\mathrm{E2}] = 2\Pr(G\cap A_h = \emptyset, D_i\cap C\cap G\neq\emptyset, D_i\cap\partial C\neq\emptyset) + \Pr(G\cap L_h\neq\emptyset, D_i\cap\partial C\neq\emptyset)$$

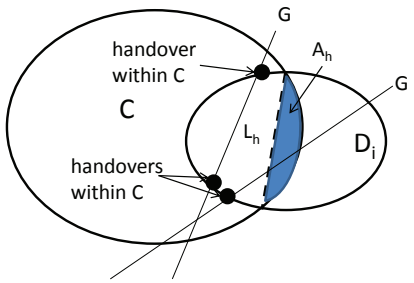

Fig. 6. A_h and L_h

$$
\begin{aligned}
&= \frac{\int_{D_i\cap\partial C\neq\emptyset}\{2\int_{D_i\cap C\cap G\neq\emptyset} dG - 2\int_{G\cap A_h\neq\emptyset} dG + \int_{G\cap L_h\neq\emptyset} dG\}dD_i}{\int_{C\cap G\neq\emptyset, C\cap D_i\neq\emptyset} dG\ dD_i} \\
&= \frac{\int_{D_i\cap\partial C\neq\emptyset}(2|D_i\cap C| - 2|A_h| + |L_h|)dD_i}{\int_{C\cap G\neq\emptyset, C\cap D_i\neq\emptyset} dG\ dD_i} \\
&= \frac{\int_{D_i\cap\partial C\neq\emptyset} 2l_{\partial D_i\cap C}dD_i}{\int_{C\cap G\neq\emptyset, C\cap D_i\neq\emptyset} dG\ dD_i}.
\end{aligned} \tag{66}
$$

Because D_j $(j\neq i)$ is independent of G and D_i,

$$
N_h = \sum_{i=1}^{l}(E[S_i|\mathrm{E1}] + E[S_i|\mathrm{E2}])\Pr((G\cap\partial D_i)\notin\bigcup_{j\neq i} D_j|\{C\cap D_j\neq\emptyset\}_{j\neq i}) \tag{67}
$$

where $\Pr((G\cap\partial D_i)\notin\bigcup_{j\neq i} D_j|\{C\cap D_j\neq\emptyset\}_{j\neq i})$ is a conditional probability that an intersection between G and ∂D_i is not covered by any of D_j $j\neq i$ with the condition that $\{C\cap D_j\neq\emptyset\}_{j\neq i}$.

Then, we can derive the following result.

Result 12: For a homogeneous Poisson process,

$$
N_h = \sum_{i=1}^{l}\frac{4\pi\|C\|\cdot|D_i|}{|C|f(C,D_i)}\Pr((G\cap\partial D_i)\notin\bigcup_{j\neq i} D_j|\{C\cap D_j\neq\emptyset\}_{j\neq i}). \tag{68}
$$

For an inhomogeneous Poisson process

$$
N_h \approx \sum_{i=1}^{l}\frac{4\pi(\|C\| + \rho_H\|C\cap\Omega_H\| - \rho_L\|C\cap\Omega_L\|)}{g_1(C,D_i)|C|}|D_i|\Pr((G\cap\partial D_i)\notin\bigcup_{j\neq i} D_j|\{C\cap D_j\neq\emptyset\}_{j\neq i}). \tag{69}
$$

Proof of Eq. (68): Assume a homogeneous Poisson process. Due to Eqs. (1) and (5),

$$
\int_{D_i\subset C, D_i\cap G\neq\emptyset} dG\,dD_i = \int_{D_i\subset C}|D_i|dD_i = |D_i|\{2\pi(\|D_i\| + \|C\|) - |D_i|\cdot|C|\}, \tag{70}
$$

and due to Eqs. (1) and (3),

$$
\int_{C\cap G\neq\emptyset, C\cap D_i\neq\emptyset} dG\ dD_i = |C|f(C,D_i). \tag{71}
$$

Apply these two equations to Eq. (65).

Due to Eq. (7),

$$
\int_{D_i\cap\partial C\neq\emptyset} l_{\partial D_i\cap C}dD_i = |D_i|(|C|\cdot|D_i| - 2\pi\|D_i\|). \tag{72}
$$

Apply this equation to Eq. (66). Therefore, we obtain Eq. (68). □

Proof of Eq. (69): Assume an inhomogeneous Poisson process. According to Eqs. (1), (5), (10), and (23) with $\phi = 1, X_c = D_i\subset C$,

$$
\begin{aligned}
&\int_{D_i\cap G\neq\emptyset, D_i\subset C} dG\,dD_i \\
\approx\ & \rho_0|D_i|\{\int_{D_i\subset C,\mathbf{w}_i\in\mathbb{R}^2} d\mathbf{w}_i\ d\gamma_i + \rho_H\int_{D_i\subset C,\mathbf{w}_i\in\Omega_H} d\mathbf{w}_i\ d\gamma_i - \rho_L\int_{D_i\subset C,\mathbf{w}_i\in\Omega_L} d\mathbf{w}_i\ d\gamma_i\}
\end{aligned}
$$

$$\approx \quad \rho_0 g_3(C, D_i) \tag{73}$$

where $g_3(C, D_i) \stackrel{\text{def}}{=} |D_i|\{2\pi(\|D_i\|+\|C\|)-|D_i|\cdot|C|+2\pi\rho_H(\|C\cap\Omega_H\|-\hat{r}(D_i)l_{\partial C\cap\Omega_H})-2\pi\rho_L(\|C\cap\Omega_L\|-\hat{r}(D_i)l_{\partial C\cap\Omega_L})\}$. Apply this equation and Eqs. (1) and (24) to Eq. (65).

Due to Eqs. (7), (14), and (23) with $\phi = l_{\partial D_i\cap C}, X_c = D_i \cap \partial C \neq \emptyset$,

$$\begin{aligned} & \int_{D_i\cap\partial C\neq\emptyset} l_{\partial D_i\cap C} dD_i \\ = \quad & \rho_0\{\int_{D_i\cap\partial C\neq\emptyset, \mathbf{w}_i\in\mathbb{R}^2} l_{\partial D_i\cap C} d\mathbf{w}_i \; d\gamma_i + \rho_H \int_{\partial C\cap D_i\neq\emptyset, \mathbf{w}_i\in\Omega_H} l_{\partial D_i\cap C} d\mathbf{w}_i \; d\gamma_i \\ & -\rho_L \int_{\partial C\cap D_i\neq\emptyset, \mathbf{w}_i\in\Omega_L} l_{\partial D_i\cap C} d\mathbf{w}_i \; d\gamma_i\} \\ \approx \quad & \rho_0|D_i|\{(|C|\cdot|D_i| - 2\pi\|D_i\|) + 2\pi\rho_H\hat{r}(D_i)l_{\partial C\cap\Omega_H} - 2\pi\rho_L\hat{r}(D_i)l_{\partial C\cap\Omega_L}\}. \end{aligned} \tag{74}$$

Apply this equation and Eqs. (1) and (24) to Eq. (66). As a result, we obtain Eq. (69). □

Now, we need to evaluate $\Pr((G\cap\partial D_i) \notin \bigcup_{j\neq i} D_j | \{C\cap D_j\neq\emptyset\}_{j\neq i}) = \frac{\int_{(G\cap\partial D_i)\notin\bigcup_{j\neq i} D_j, \{C\cap D_j\neq\emptyset\}_{j\neq i}} ((dD)^l/dD_i)}{\int_{\{C\cap D_j\neq\emptyset\}_{j\neq i}} ((dD)^l/dD_i)}$ where where $((dD)^l/dD_i) \stackrel{\text{def}}{=} dD_1\cdots dD_{i-1}\, dD_{i+1}\cdots dD_l$.

Result 13: For a homogeneous Poisson process,

$$\Pr((G\cap\partial D_i) \notin \bigcup_{j\neq i} D_j | \{C\cap D_j\neq\emptyset\}_{j\neq i}) = \Pi_{j\neq i}(1 - 2\pi\|D_j\|/f(C, D_j)). \tag{75}$$

For an inhomogeneous Poisson process,

$$\Pr((G\cap\partial D_i) \notin \bigcup_{j\neq i} D_j | \{C\cap D_j\neq\emptyset\}_{j\neq i}) \approx \Pi_{j\neq i}(1 - 2\pi\|D_j\| g_4(C)/g_1(C, D_j)) \tag{76}$$

where $g_4(C) \stackrel{\text{def}}{=} 1 + (\rho_H\lambda_H\|C\cap\Omega_H\| - \rho_L\lambda_L\|C\cap\Omega_L\|)/(\lambda_C\|C\|)$.

Proof: Note that $\int_{(G\cap\partial D_i)\notin D_j, C\cap D_j\neq\emptyset} dD_j = \int_{(G\cap\partial D_i)\notin D_j, C\cap D_j\neq\emptyset} dD_j = \int_{C\cap D_j\neq\emptyset} dD_j - \int_{(G\cap\partial D_i)\in D_j} dD_j$, because $(G\cap\partial D_i)\subset C$.

Therefore, for a homogeneous Poisson process, due to Eqs. (3) and (4), for $j\neq i$,

$$\int_{(G\cap\partial D_i)\notin D_j, C\cap D_j\neq\emptyset} dD_j = f(C, D_j) - 2\pi\|D_j\|, \tag{77}$$

By repeatedly using Eqs. (3) and (77),

$$\Pr((G\cap\partial D_i) \notin \bigcup_{j\neq i} D_j | \{C\cap D_j\neq\emptyset\}_{j\neq i}) = \Pi_{j\neq i}(1 - 2\pi\|D_j\|/f(C, D_j)). \tag{78}$$

For an inhomogeneous Poisson process, due to Eqs. (23) with $\phi = 1, X_c = (G\cap\partial D_i)\in D_j$ and (24),

$$\begin{aligned} & \int_{(G\cap\partial D_i)\notin D_j, D_j\cap C\neq\emptyset} dD_j \\ \approx \quad & \rho_0 g_1(C, D_j) \\ & -\rho_0\{\int_{(G\cap\partial D_i)\in D_j, \mathbf{w}_i\in\mathbb{R}^2} d\mathbf{w}_i \; d\gamma_i + \rho_H \int_{(G\cap\partial D_i)\in D_j, \mathbf{w}_i\in\Omega_H} d\mathbf{w}_i \; d\gamma_i - \rho_L \int_{(G\cap\partial D_i)\in D_j, \mathbf{w}_i\in\Omega_L} d\mathbf{w}_i \; d\gamma_i\} \\ \approx \quad & \rho_0 g_1(C, D_j) - 2\pi\rho_0\|D_j\|\{1 + \rho_H \Pr((G\cap\partial D_i)\in\Omega_H) - \rho_L \Pr((G\cap\partial D_i)\in\Omega_L)\}. \end{aligned} \tag{79}$$

The last equality above is due to Eqs. (4) and (11).

It is reasonable to assume that $\Pr((G\cap\partial D_i)\in\Omega_H)$ ($\Pr((G\cap\partial D_i)\in\Omega_L)$) is proportional to the ratio of the mean number of WLANs in $\Omega_H\cap C$ ($\Omega_L\cap C$) to that in C. That is, assume that $\Pr((G\cap\partial D_i)\in\Omega_H) \approx \frac{\lambda_H\|C\cap\Omega_H\|}{\lambda_H\|C\cap\Omega_H\|+\lambda_L\|C\cap\Omega_L\|+\lambda_0(\|C\|-\|C\cap\Omega_H\|-\|C\cap\Omega_L\|)} = \frac{(1+\rho_H)\|C\cap\Omega_H\|}{\|C\|+\rho_H\|C\cap\Omega_H\|-\rho_L\|C\cap\Omega_L\|} = \lambda_H\|C\cap\Omega_H\|/(\lambda_C\|C\|)$, and $\Pr((G\cap\partial D_i)\in\Omega_L) \approx \lambda_L\|C\cap\Omega_L\|/(\lambda_C\|C\|)$. Therefore,

$$\int_{(G\cap\partial D_i)\notin D_j, D_j\cap C\neq\emptyset} dD_j \quad \approx \quad \rho_0(g_1(C, D_j) - 2\pi\|D_j\| g_4(C)). \tag{80}$$

By repeatedly applying this equation and Eq. (24),

$$\Pr((G\cap\partial D_i) \notin \bigcup_{j\neq i} D_j | \{C\cap D_j\neq\emptyset\}_{j\neq i}) \approx \Pi_{j\neq i}(1 - 2\pi\|D_j\| g_4(C)/g_1(C, D_j)). \tag{81}$$

Consequently, we obtain the following result.

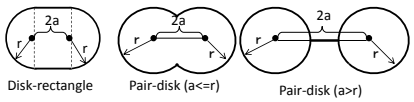

Fig. 7. Shape of D

Result 14: The mean number N_h of vertical handovers is approximately given by the following formula under an inhomogeneous Poisson process.

$$N_h \approx \frac{4\pi \sum_{i=1}^{l} |D_i|(\|C\| + \rho_H \|C \cap \Omega_H\| - \rho_L \|C \cap \Omega_L\|)\Pi_{j \neq i}(g_1(C, D_j) - 2\pi \|D_j\| g_4(C))}{|C| \Pi_{i=1}^{l} g_1(C, D_i)} \tag{82}$$

Under a homogeneous Poisson process, this approximation formula becomes exact and simplified into

$$N_h = \frac{4\pi \|C\| \sum_{i=1}^{l} |D_i| \Pi_{j \neq i}(f(C, D_j) - 2\pi \|D_j\|)}{|C| \Pi_{i=1}^{l} f(C, D_i)}. \tag{83}$$

VII. Numerical examples

A. Conditions of numerical examples

In the numerical examples in this section, we assume that all D_i are congruent for any i and are disk-rectangles or pair-disks, as shown in Fig. 7, with $r = 50$ m (disk-shaped D means $a = 0$). We set $r = 50$ m based on a measurement study [30] or information [31] where the range of WiFi APs is reported as dozens of meters to over 100 m.

To determine the parameter setting of bitrates s_i for cellular networks and s_w for WLANs, we use the results of measurement studies in actually operated WiFi and 3G networks [32], [33], [34]. They measured throughput from a server with a public IP address to mobile terminal(s) with a WiFi interface and that with a 3G interface under various access scenarios such as walking or driving for a long/short distance. Deshpande et al. [32] used a commercially operated metro-scale WiFi network while Balasubramanian et al. [33] and Gass and Diot [34] used open WiFi APs in the wild. In [32], [33], [34], the measured throughput of the WLAN ranged from $1 - 2$ (Mbps) at median or average to around $5 - 10$ (Mbps) at maximum. For 3G networks, the throughput ranged from about 500 (kbps) at median or average to around $1.5 - 2$ (Mbps) at maximum. Another performance metric is availability. Balasubramanian et al. [33] reported that the availability of the 3G network is 87% while that of the WiFi network is 11%. Because of the low availability of WiFi, the median or average throughput becomes small, so in our numerical example, we use the maximum throughput of WiFi as the bitrate of a WLAN cell $s_w = 10,000$ (kbps) rather than average or median of throughput, assuming that the offloading is executed when the terminal moves into a WLAN cell and is expected to achieve sufficient throughput. (The throughput measurement studies of a WLAN network in experimental environments, such as [30], [35], show that the maximum throughput is about $10 - 20$ (Mbps).)

For cellular network parameters, we use the distribution of throughput in [32] as follows. Assuming that a user location is uniformly distributed in a cell, we first calculate the frequency (in percentage) F_i of users existing in $C_i - C_{i+1}$ where C_i are disk-shaped with radii $1000, 500, 200, 100$ (m) for $i = 1, 2, 3, 4$. For example, $F_4 = 100^2/1000^2 \times 100 = 1\%$ and $F_3 = (200^2 - 100^2)/1000^2 \times 100 = 3\%$. We also assume that the throughput, i.e., the achieved bitrate (bps) s_i, in $C_i - C_{i+1}$ is higher than s_{i-1}. We set $s_i (i = 1, 2, 3)$ so that the s_i is between the $100 - \sum_{j=i}^{4} F_j$ and $100 - \sum_{j=i+1}^{4} F_j$ percentile of throughput, i.e., s_i is set to the $100 - (\sum_{j=i}^{4} F_j + \sum_{j=i+1}^{4} F_j)/2$ percentile. For s_4, we set s_4 to be the $100 - F_4/2$ percentile of throughput. Based on the graph in [32], we set $s_1 = 300$, $s_2 = 750$, $s_3 = 1500$, and $s_4 = 2000$ (kbps).

B. Accuracy of proposed formulas

We compare the values of the performance metrics derived by the derived formulas and those obtained by simulation, where the empirical data of the WLAN APs of three network operators are used. We provide the center of C at one of the nine 1200 $\times$ 1200-m square grids in which the upper left corner is located at (1200 m, -1200 m) on the map in Fig. 1. For this location of C, we conducted simulation. Because we change the location of C to another one of the nine grids, we can obtain nine simulation results for each operator.

To evaluate the metric theoretically, Ω_H and Ω_L used here are identified using the following method. (1) Divide the 5 $\times$ 5-km square region into 100 $\times$ 100-m subregions called atoms, and set $\omega_H = \omega_L = \emptyset$. (2) Count the number of WLAN APs in each atom. Let a_0 be the average number of WLAN APs in an atom. (3) Consider a window defined by consecutive $n_0 \times n_0$ atoms. Let n_b be the number of WLAN APs in a window and a_U and a_L be the 0.999 upper/lower quantile of n_b under a homogeneous Poisson process: $a_U \stackrel{\text{def}}{=} a_0 n_0^2 + 3\sqrt{a_0} n_0$ and $a_L \stackrel{\text{def}}{=} a_0 n_0^2 - 3\sqrt{a_0} n_0$. If $n_b > a_U$ ($n_b < a_L$), atoms in the window are determined as atoms in ω_H (ω_L). (4) Slide the window and repeat (3) until the window sweeps the entire 5 $\times$

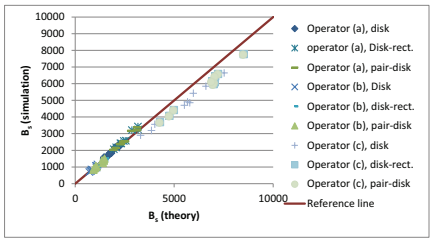

Fig. 8. Comparison between theory and simulation for B_s

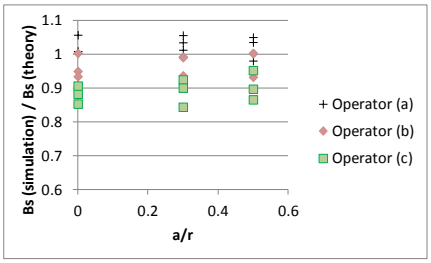

Fig. 9. Ratio of B_s derived by simulation to that derived by theory for pair-disk shaped C_i

5-km square region. (5) Atoms belonging to ω_H (ω_L) more than $n_0^2/2$ times are determined as those belonging to Ω_H (Ω_L). Note that Ω_H (Ω_L) may not be consecutive.

In this paper, the set of WLAN AP data of operator (c) is used to identify Ω_H and Ω_L because the number of APs is much larger than those of the other operators. We used $n_0 = 3$. As a result, we obtained $\|\Omega_H\| = 3.48$ km^2, $\|\Omega_L\| = 5.31$ km^2; λ_0=23.87, λ_H=27.30, λ_L=4.33, ρ_H=0.143, and ρ_L=0.819, for operator (a); λ_0=5.305, λ_H=20.40, λ_L=1.318, ρ_H=2.846, and ρ_L=0.752, for operator (b); and λ_0=103.8, λ_H=575, λ_L=3.766, ρ_H=4.538, and ρ_L=0.964, for operator (c). In addition to these parameter values, we obtained the number l of WLANs intersecting C, $\|C_j \cap \Omega_H\|$, $\|C_j \cap \Omega_L\|$, $l_{\partial C \cap \Omega_H}$, and $l_{\partial C \cap \Omega_L}$ in the simulation, and used them in the theoretical evaluation.

Figure 8 shows the comparison results for B_s. Each point corresponds to each location of C. Although there is a small bias for operator (c), the agreement between the theoretical and simulation results is, in general, very good. Therefore, we conclude that the derived approximation formula works fine.

We also investigated the accuracy of the proposed model for a non-convex C_i. C_i is assumed to be pair-disk shaped (Fig. 7) for all i and the middle points of two disk centers for all i are located at the same point. The line between two disk centers of C_i is parallel to the x-axis in Fig. 1. Figure 9 plots the ratio of B_s derived by simulation to that derived by theory where the x-axis denotes the ratio a/r in Fig. 7 and each point in this figure corresponds to the locations of the middle point of two disk centers of C_i. This figure shows that there is no clear accuracy deterioration, although a pair-disk with $a/r > 0$ is not convex.

We also simulated B_d by drawing 1000 lines as G for each case and compared 27 cases of B_s and B_d (nine locations of the center of C and three shapes for D) for each operator. The relative absolute difference $|B_d - B_s|/B_d$ was at most 3.23%, 3.38%, and 2.48%, and the average was 1.51%, 1.59%, and 0.640% for operators (a), (b), and (c). Therefore, we can say that $B_d = B_s$ is valid. As a result, our derived approximation formula also works fine for B_d because it works fine for B_s.

Figure 10 compares N_v derived using the derived formula and the simulation. For operators (a) and (b), the theoretical and simulation results agree well. On the contrary, the derived formula largely underestimates N_v in most cases for operator (c). This is because l (the number of WLANs intersecting C) of operator (c) is much larger than 100 and is sometimes larger than 1000, and because Eq. (82) includes the product term $(1 - \frac{2\pi\|D_j\|g_4(C)}{g_1(C,D_j)})^l$. When there is a small approximation error or modeling error in $1 - \frac{2\pi\|D_j\|g_4(C)}{g_1(C,D_j)}$, the error becomes enormous in N_v. For example, when $l = 1000$, $0.99^l/0.98^l \approx 2.5 \times 10^4$. That is, the difference of 1% results in a difference of four orders of magnitude. Because l for operator (a) is nearly 100, and that for operator (b) is much less than 100, we need to be careful when using the derived formula for $l \gg 100$.

C. Evaluation of metrics

In the remainder of this paper, the following are the parameter values we use in the evaluation in addition to those described at the beginning of this section, unless explicitly indicated otherwise. These parameter values are called the default values: $\|C \cap \Omega_H\| = \|C \cap \Omega_L\| = 0.3\|C\|$, $a = 0$ (that is, D is disk-shaped), $\rho_H = 3$, $\rho_L = 1$, $l_{\partial C \cap \Omega_H} = 2\sqrt{2\|C \cap \Omega_H\|/\pi}$, and

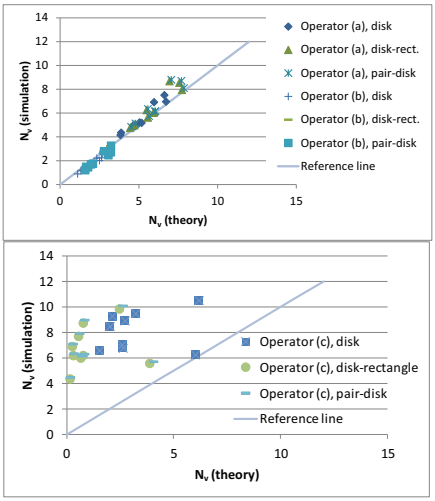

Fig. 10. Comparison between theory and simulation for N_v

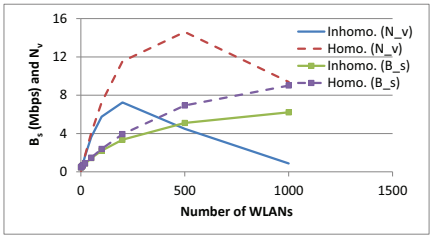

Fig. 11. Comparison between inhomogeneous Poisson process and homogeneous Poisson process for B_s and N_v

$l_{\partial C\cap\Omega_L} = 2\sqrt{2\|C\cap\Omega_L\|/\pi}$. The default values of $l_{\partial C\cap\Omega_H}$ and $l_{\partial C\cap\Omega_L}$ are based on the assumption that $C\cap\Omega_H$ ($C\cap\Omega_L$) is a semicircle and $l_{\partial C\cap\Omega_H}$ ($l_{\partial C\cap\Omega_L}$) is its diameter.

First, we compare $B_s(=B_d)$ and N_v under the inhomogeneous Poisson process with the default parameter values and those under the homogeneous Poisson process. The results are plotted in Fig. 11. As l (the number of WLANs) increases, the difference in B_s under these processes becomes quite large. When $l=1000$, B_s under the homogeneous Poisson process is overestimated by about 50% compared to B_s under the inhomogeneous Poisson process. Furthermore, (1) N_v is not monotone against l, and (2) N_v under the homogeneous Poisson process is extremly overestimated compared to N_v under the inhomogeneous Poisson process. Fact (2) is natural because $\{D_i\}_i$ under the inhomogeneous Poisson process is more likely to clump than that under the homogeneous Poisson process. Therefore, $\{D_i\}_i$ is likely to make a cluster, and the vertical handover does not occur in a cluster of $\{D_i\}_i$.

We also compare r_{WLAN} (the ratio in which the traffic is delivered through the WLANs) and p_{WLAN}(the raito of C covered by WLANs) under the inhomogeneous Poisson process with the default parameter values and those under the homogeneous Poisson process. Assume that traffic is uniformly generated in C. If the point where traffic is generated is covered by a WLAN AP, the traffic is assumed to be delivered through the WLAN with achieved bitrate s_w (bps); otherwise, it is delivered through the cellular network with achieved bitrate $s_1,\cdots,s_n$ (bps). The ratio r_{WLAN} is approximately given by $s_w(1-\sum_{j=1}^{n}(b_0g_0(j)+b_Hg_H(j)+b_Lg_L(j))/\|C\|)/B_s$. Similarly, the ratio p_{WLAN} is approximately given by $\sum_{j=1}^{n}p_j \approx 1-\sum_{j=1}^{n}(b_0g_0(j)+b_Hg_H(j)+b_Lg_L(j))/\|C\|$.

Figure 12 shows r_{WLAN} and p_{WLAN}. The former approaches 1 very fast because the difference in s_w and s_i is very large. The difference in "Inhomogeneous" and "Homogeneous" is not negligible. On the other hand, the latter is similar to the curve of B_s in Fig. 11. As the number l of WLANs increases, p_{WLAN} becomes larger. However, its increase becomes smaller as l becomes larger.

Second, we evaluate the impact of ρ_H and ρ_L on B_s and N_v (Figs. 13, 14). When $l=100$, $B_s(=B_d)$ is almost insensitive to ρ_H or ρ_L. When $l=500$, B_s decreases as ρ_H or ρ_L increases. N_v is also a decreasing function of ρ_H and ρ_L. The sensitivity of N_v to ρ_H or ρ_L becomes larger as l increases. Because ρ_H and ρ_L indicate the relative difference in λ_H and λ_L from λ_0, this means that B_s and N_v become smaller when inhomogeneity becomes larger.

The values $\|C\cap\Omega_H\|$ and $\|C\cap\Omega_L\|$ are clump parameters of the spatial point process of deployed WLANs. Figure 15

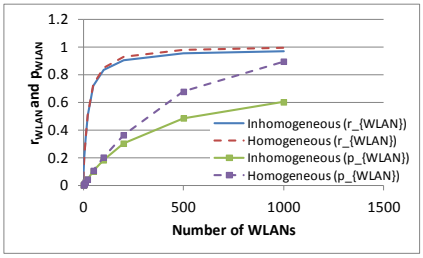

Fig. 12. Ratio in which traffic is delivered through WLANs and ratio of C covered by WLANs.

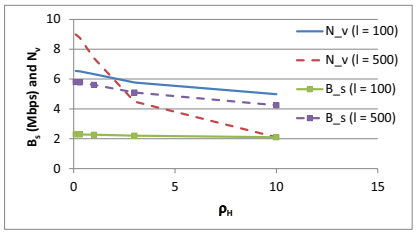

Fig. 13. Impact of ρ_H on B_s and N_v

plots $B_s(=B_d)$ and N_v as a function of $\|C\cap\Omega_H\|/\|C\|$ or $\|C\cap\Omega_L\|/\|C\|$. Because the default value of $\|C\cap\Omega_H\|/\|C\|$ ($\|C\cap\Omega_L\|/\|C\|$) is 0.3, $\|C\cap\Omega_L\|/\|C\|$ ($\|C\cap\Omega_H\|/\|C\|$) can move from 0 to 0.7. In this figure, B_s and N_v are decreasing functions of $\|C\cap\Omega_L\|/\|C\|$. This is because when the low WLAN-density region (Ω_L) becomes larger in C with a fixed l, many WLAN APs must be in the high or normal WLAN-density region (Ω_H, $\overline{\Omega_H\cup\Omega_L}$), mainly in Ω_H. As a result, $\{D_i\}_i$ overlap each other in such regions, particularly in Ω_H. The lower B_s means that $\{D_i\}_i$ cannot achieve efficient coverage due to this overlap, and the smaller N_v is also due to this overlap. On the other hand, either B_s or N_v is not monotonous against $\|C\cap\Omega_H\|/\|C\|$ and has the minimum point between $\|C\cap\Omega_H\|/\|C\|=0$ and 0.7. This is because (i) when $\|C\cap\Omega_H\|/\|C\|=0$, WLAN APs are in the normal density region, which occupies 70% of C. Thus, $\{D_i\}_i$ do not overlap so much. (ii) When $0<\|C\cap\Omega_H\|/\|C\|<0.7$, $\{D_i\}_i$ overlap each other in Ω_H and $\overline{\Omega_H\cup\Omega_L}$, particularly in Ω_H. Because of the overlaps, efficient coverage cannot be achieved or vertical handover does not occur. (iii) When $\|C\cap\Omega_H\|/\|C\|=0.7$, WLAN APs are in $\Omega_H\cap C$ but $\{D_i\}_i$ do not overlap so much because $\Omega_H\cap C$ occupies 70% of C. For $l=500$, B_s is more sensitive to $\|C\cap\Omega_L\|/\|C\|$ than to ρ_L, and more sensitive to ρ_H than to $\|C\cap\Omega_H\|/\|C\|$. (Although ρ_H is in [0,10) in Fig. 13, the range of ρ_H is $[0,\infty)$. Even in $\rho_H\in[0,10)$, the range of B_s shown in Fig. 13 is larger than that of B_s for the full range of $\|C\cap\Omega_H\|/\|C\|$.) Therefore, $\|C\cap\Omega_L\|/\|C\|$ and ρ_H are important parameters for B_s. N_v is also more sensitive to $\|C\cap\Omega_L\|/\|C\|$ than to ρ_L, and to ρ_H than to $\|C\cap\Omega_H\|/\|C\|$. Thus, $\|C\cap\Omega_L\|/\|C\|$ and ρ_H are also important parameters for N_v.

Figure 16 plots $B_s(=B_d)$ and N_v as functions of $l_{\partial C\cap\Omega_H}$ and $l_{\partial C\cap\Omega_L}$. It shows that B_s is a slightly increasing function of $l_{\partial C\cap\Omega_H}$ and a slightly decreasing function of $l_{\partial C\cap\Omega_L}$. However, B_s is more sensitive to other parameters such as $\|C\cap\Omega_L\|/\|C\|$ and ρ_H. The behavior of N_v as a function of $l_{\partial C\cap\Omega_H}$ and $l_{\partial C\cap\Omega_L}$ is interesting. When $l=100$, it is an increasing function of $l_{\partial C\cap\Omega_H}$ and a decreasing function of $l_{\partial C\cap\Omega_L}$. However, when $l=500$, it is the opposite: it is a decreasing function of $l_{\partial C\cap\Omega_H}$ and an increasing function of $l_{\partial C\cap\Omega_L}$. As a whole, N_v is more sensitive to other parameters such as $\|C\cap\Omega_L\|/\|C\|$

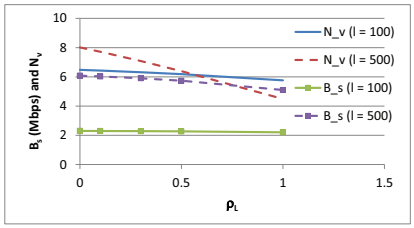

Fig. 14. Impact of ρ_L on B_s and N_v

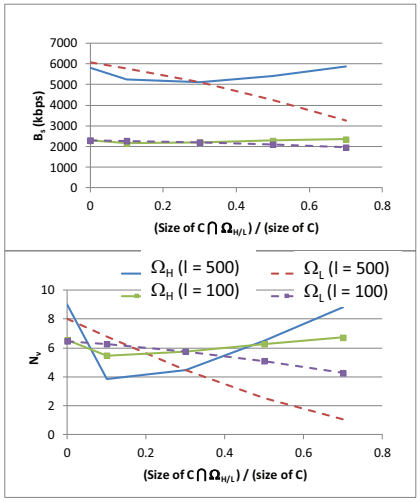

Fig. 15. Impact of $\|C \cap \Omega_H\|$ and $\|C \cap \Omega_L\|$ on B_s and N_v

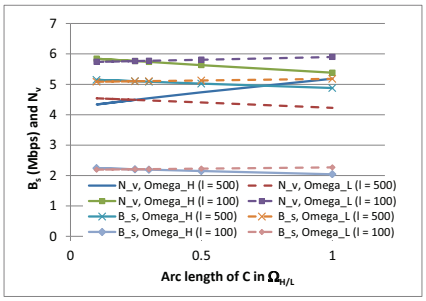
B_s (Mbps) and N_v
N_v, Omega_H (l = 500)
N_v, Omega_L (l = 500)
N_v, Omega_H (l = 100)
N_v, Omega_L (l = 100)
B_s, Omega_H (l = 500)
B_s, Omega_L (l = 500)
B_s, Omega_H (l = 100)
B_s, Omega_L (l = 100)
Arc length of C in $\Omega_{H/L}$

Fig. 16. Impact of $l_{\partial C \cap \Omega_H}$ and $l_{\partial C \cap \Omega_L}$ on B_s and N_v

and ρ_H.

Finally, we investigate the impact of the shape of D on $B_s (= B_d)$ and N_v for fixed $\|D\|$. (As a result, a is variable while r is given.) Figure 17 shows the results. For disk-rectangular D and for pair-disk shaped D, B_s is not very sensitive to the shape of D. N_v is more sensitive to the shape of D than B_s. This is because the length of D as well as its size has a large impact on N_v, although B_s is mainly determined by the size of D. N_v becomes minimum at $a = 0$, that is, when D is disk-shaped. The difference in N_v for disk-rectangles and for pair-disks becomes noticeable around $a \approx r$. This is because $|D|$ of a disk-rectangle D becomes significantly different from that of a pair-disk D when $a \gtrapprox r$.

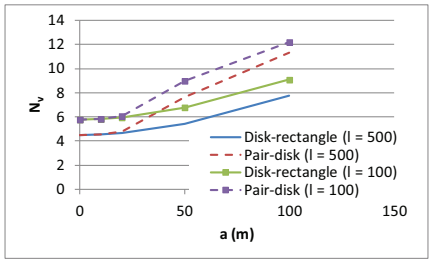

Fig. 17. Impact of the shape of D on B_s and N_v

VIII. Conclusion

We analyzed empirical data of the locations of WLAN APs and proposed an inhomogeneous Poisson process as a location model. Based on the proposed model, explicit formulas for performance metrics, such as bandwidth (speed) available to users, were derived through integral geometry. The derived formulas show good agreement with the simulation results using the empirical data. They are exact under a homogeneous Poisson process. We proved that the static available bandwidth and the dynamic available bandwidth are the same as a probabilistic distribution under a homogeneous Poisson process, and that their approximated probability are also the same when $\|D_i\| = \|D\|$ and $|D_i| = |D|$ for all i even under an in homogeneous Poisson process. These facts strongly suggest that the bandwidth experienced by a user is not dependent on user mobility.

Because these performance metrics depend on many parameters, such as the number of WLAN APs, the shape of each WLAN coverage region, the location of each WLAN AP, the available bandwidth (bps) of a WLAN, and the shape and available bandwidth (bps) of each subregion identified by the channel quality indicator in a cell of the cellular network, it is difficult to cover all the cases through computer simulation. Therefore, the derived formulas are useful tools for performance evaluation of offloading through WLANs.

Numerical examples based on the derived formulas show the following: (1) A homogeneous Poisson process can be too optimistic concerning the performance metrics such as user bandwidth (speed). (2) Parameters, such as the size of regions where placement of WLAN APs is not allowed and the mean density of WLANs in high density regions, have a large impact on the performance metrics.

The analysis method used in this paper and some basic formulas derived in this paper are potentially applicable to other applications. Actual applicability to other aplications will be investigated in the future.

References

[1] Y. Choi, H. W. Ji, J.-Y, Park, H.-C Kim, and J. A. Silvester, A 3W Network Strategy for Mobile Data Traffic Offloading, IEEE Communications Magazine, 49, 10, pp. 118-123, 2011.
[2] A. de la Oliva, C. J. Bernardos, M. Calderon, T. Melia, and J. C. Zuniga, IP Flow Mobility: Smart Traffic Offload for Future Wireless Networks, IEEE Communications Magazine, 49, 10, pp. 124-132, 2011.
[3] C. B. Sankaran, Data Offloading Techniques in 3GPP Rel-10 Networks: A Tutorial, IEEE Communications Magazine, 50, 6, pp.46-53, 2012.
[4] Noel A. C. Cressie, Statistics for Spatial Data, John Wiley & Sons, 1991.
[5] B. D. Ripley, Spatial Statistics, John Wiley & Sons, 1981.
[6] S. Mase and J. Takeda, Spatial Data Modeling, Kyoritsu, 2001 (in Japanese).
[7] A. Baddeley and R. Turner, spatstat: An R Package for Analyzing Spatial Point Patterns, Journal of Statistical Software, 12, 6, 2005.
[8] J. Riihijärvi and P. Mähönen, and M. Rübsamen, Characterizing Wireless Networks by Spatial Correlations, IEEE Communication Letters 2007.
[9] J. Riihijärvi and P. Mähönen, Modeling Spatial Structure of Wireless Communication Networks, NetSciCom 2010, 2010.
[10] M. Michalopoulou, J. Riihijärvi and P. Mähönen, Studying the Relationships between Spatial Structures of Wireless Networks and Population Densities, IEEE Globecom 2010.
[11] J. G. Andrews, F. Baccelli, R. K. Ganti, A Tractable Approach to Coverage and Rate in Cellular Networks, IEEE Transactions on Communications 59, 11, pp. 3122-3134, 2011.
[12] C. Gloaguen, F. Voss, and V. Schmidt, Parametric Distance Distributions for Fixed Access Network Analysis and Planning, 21st International Teletraffic Congress (ITC21), Paris, 2011.
[13] C. Gloaguen, H. Schmidt, R. Thiedmannz, J. Lanquetiny, and V. Schmidt, Comparison of Network Trees in Deterministic and Random Settings using Different Connection Rules, Modeling and Optimization in Mobile, Ad Hoc and Wireless Networks and Workshops, 2007.
[14] H. Saito, K. Shimogawa, S. Shioda, and J. Harada, Shape Estimation Using Networked Binary Sensors, INFOCOM 2009, 2009.
[15] H. Saito, S. Tanaka, and S. Shioda, Estimating Parameters of Multiple Heterogeneous Target Objects Using Composite Sensor Nodes, IEEE Trans. Mobile Computing, 11, 1, pp. 125-138, 2012.
[16] H. Saito, S. Tanaka, and S. Shioda, Stochastic Geometric Filter and its Application to Shape Estimation for Target Objects, IEEE Trans. Signal Processing, 59, 10, pp. 4971-4984, 2011.
[17] L. Lazos, R. Poovendran, and J. A. Ritcey, Probabilistic Detection of Mobile Targets in Heterogeneous Sensor Networks, IPSN07, pp. 519–528, 2007.
[18] L. Lazos and R. Poovendran, Stochastic Coverage in Heterogeneous Sensor Networks, ACM Transactions on Sensor Networks, 2, 3, pp. 325–358, 2006.
[19] L. A. Santaló, Integral Geometry and Geometric Probability, Second edition. Cambridge University Press, Cambridge, 2004.
[20] S. Kwon and N. B. Shroff, Analysis of Shortest Path Routing for Large Multi-Hop Wireless Networks, IEEE/ACM Trans. Networking, 17, 3, pp. 857–869, 2009.
[21] W. Choi and S. K. Das, A Novel Framework for Energy-Conserving Data Gathering in Wireless Sensor Networks, INFOCOM 2005, pp. 1985–1996, 2005.
[22] S. Neumayer and E. Modiano, Network Reliability With Geographically Correlated Failures, INFOCOM 2010, 2010.
[23] H. Saito, Disaster Evaluation Model for Networks and its Analysis, submitted for publication.
[24] livedoor public wireless LAN internet access service site (in Japanese): http://wireless.livedoor.com/map/ [Last access: 2 Oct., 2013].
[25] NTT East FLET's public wireless LAN internet access service site (in Japanese): http://flets.com/spot/ap/ap_search_s.html [Last access: 2 Oct., 2013].
[26] SoftBank public wireless LAN internet access service site (in Japanese): http://mb.softbank.jp/mb/service_area/sws/ [Last access: 2 Oct., 2013].
[27] K. I. Pedersen, T. E. Kolding, F. Frederiksen, I. Z. Kovacs, D. Laselva, and P. E. Mogensen, An Overview of Downlink Radio Resource Management for UTRAN Long-Term Evolution, IEEE Communications Magazine, pp. 86-93, July 2009.
[28] P. Bhat, S. Nagata, L. Campoy, I. Berberana, T. Derham, G. Liu, X. Shen, P. Zong, and Jin Yang, LTE-Advanced: An Operator Perspective, IEEE Communications Magazine, pp. 104-114, February 2012.
[29] E. Dahlman, S. Parkvall, J. Skold, and P. Beming, 3G evolution: HSPA and LTE for mobile broadband (2nd edition), Elsevier, UK, 2008.
[30] J. C. Chen and J. M. Gilbert, Measured Performance of 5-GHz 802.11a Wireless LAN Systems: http://www.iet.unipi.it/f.giannetti/documenti/wlan/Data/refer/AtherosRangeCapacityPaper.pdf [Last access: 4 Oct., 2013]
[31] http://en.wikipedia.org/wiki/Wi-Fi
[32] P. Deshpande, X. Hou, and S. R. Das, Performance Comparison of 3G and Metro-Scale WiFi for Vehicular Network Access, ACM IMC 2010.
[33] A. Balasubramanian, R. Mahajan, and A. Venkataramani, Augmenting Mobile 3G Using WiFi, ACM MobiSys Conference, 2010.

[34] R. Gass and C. Diot, An Experimental Performance Comparison of 3G and Wi-Fi, PAM 2010.
[35] A. L. Wijesinha, Y.-T. Song, M. Krishnan, V. Mathur, J. Ahn, and V. Shyamasundar, Throughput Measurement for UDP Traffic in an IEEE 802.11g WLAN, SNPD/SAWM 2005, May 2005.

APPENDIX

Because $C_j \cap D_{i_1} \cap D_{i_2} \cap \cdots$ is convex, by applying Eq. (24) for $i \neq i_1, \cdots, i_k$,

$$\begin{aligned} & \int_{\{C\cap D_i\neq\emptyset\}_{i=1}^l} \|C_j \cap_{m=i_1,\cdots,i_k} D_m\|(dD)^l \\ \approx\ & \Pi_{i\neq i_1,\cdots,i_k}\rho_0 g_1(C,D_i) \int_{C\cap D_{i_1}\neq\emptyset,\cdots,C\cap D_{i_k}\neq\emptyset} \|C_j \cap_{m=i_1,\cdots,i_k} D_m\| dD_{i_1}\ \cdots\ dD_{i_k} \end{aligned} \tag{84}$$

Use Eq. (23) with $\phi = \|C_j \cap_{m=i_1,\cdots,i_k} D_m\|, X_c = \{C \cap D_i \neq \emptyset\}_{i=1}^l$, and apply Eqs. (8) and (13).

$$\begin{aligned} & \int_{\{C\cap D_i\neq\emptyset\}_{i=1}^l} \|C_j \cap_{m=i_1,\cdots,i_k} D_m\| dD_{i_k} \\ =\ & \rho_0\{\int_{\{C\cap D_i\neq\emptyset\}_{i=1}^l,\mathbf{w}_{i_k}\in\mathbb{R}^2} \|C_j \cap_{m=i_1,\cdots,i_k} D_m\| d\mathbf{w}_{i_k}\ d\gamma_{i_k} \\ & +\rho_H \int_{\{C\cap D_i\neq\emptyset\}_{i=1}^l,\mathbf{w}_{i_k}\in\Omega_H} \|C_j \cap_{m=i_1,\cdots,i_k} D_m\| d\mathbf{w}_{i_k}\ d\gamma_{i_k} \\ & -\rho_L \int_{\{C\cap D_i\neq\emptyset\}_{i=1}^l,\mathbf{w}_{i_k}\in\Omega_L} \|C_j \cap_{m=i_1,\cdots,i_k} D_m\| d\mathbf{w}_{i_k}\ d\gamma_{i_k}\} \\ \approx\ & 2\pi\rho_0\|D_{i_k}\|(\|C_j \cap_{m=i_1,\cdots,i_{k-1}} D_m\| \\ & +\rho_H\|C_j \cap_{m=i_1,\cdots,i_{k-1}} D_m \cap \Omega_H\| - \rho_L\|C_j \cap_{m=i_1,\cdots,i_{k-1}} D_m \cap \Omega_L\|). \end{aligned} \tag{85}$$

Again, due to Eqs. (8), (13), and (23),

$$\begin{aligned} & \int_{\{C\cap D_i\neq\emptyset\}_{i=1}^l} \|C_j \cap_{m=i_1,\cdots,i_{k-1}} D_m \cap \Omega_H\| dD_{i_{k-1}} \\ \approx\ & 2\pi\rho_0\|D_{i_{k-1}}\|(\|C_j \cap_{m=i_1,\cdots,i_{k-2}} D_m \cap \Omega_H\| + \rho_H\|C_j \cap_{m=i_1,\cdots,i_{k-2}} D_m \cap \Omega_H\|) \\ =\ & 2\pi\rho_0(1+\rho_H)\|D_{i_{k-1}}\| \cdot \|C_j \cap_{m=i_1,\cdots,i_{k-2}} D_m \cap \Omega_H\|, \end{aligned} \tag{86}$$

because $\Omega_H \cap \Omega_H = \Omega_H$ and $\Omega_H \cap \Omega_L = \emptyset$. Therefore,

$$\begin{aligned} & \int_{\{C\cap D_i\neq\emptyset\}_{i=1}^l} \|C_j \cap_{m=i_1,\cdots,i_{k-1}} D_m \cap \Omega_H\| dD_{i_1}\cdots dD_{i_{k-1}} \\ \approx\ & \{2\pi\rho_0(1+\rho_H)\}^{k-1}\Pi_{m=1}^{k-1}\|D_{i_m}\| \cdot \|C_j \cap \Omega_H\|. \end{aligned} \tag{87}$$

Similarly,

$$\begin{aligned} & \int_{\{C\cap D_i\neq\emptyset\}_{i=1}^l} \|C_j \cap_{m=i_1,\cdots,i_{k-1}} D_m \cap \Omega_L\| dD_{i_1}\cdots dD_{i_{k-1}} \\ \approx\ & \{2\pi\rho_0(1-\rho_L)\}^{k-1}\Pi_{m=1}^{k-1}\|D_{i_m}\| \cdot \|C_j \cap \Omega_L\|. \end{aligned} \tag{88}$$

Hence,

$$\begin{aligned} & \int_{\{C\cap D_i\neq\emptyset\}_{i=1}^l} \|C_j \cap_{m=i_1,\cdots,i_k} D_m\| dD_{i_1}\ \cdots\ dD_{i_k} \\ \approx\ & 2\pi\rho_0\|D_{i_k}\| \int_{C\cap D_{i_1}\neq\emptyset,\cdots,C\cap D_{i_{k-1}}\neq\emptyset} \|C_j \cap_{m=i_1,\cdots,i_{k-1}} D_m\| dD_{i_1}\ \cdots\ dD_{i_{k-1}} \\ & +\rho_H(1+\rho_H)^{k-1}\Pi_{m=1}^k(2\pi\rho_0\|D_{i_m}\|)\|C_j \cap \Omega_H\| - \rho_L(1-\rho_L)^{k-1}\Pi_{m=1}^k(2\pi\rho_0\|D_{i_m}\|)\|C_j \cap \Omega_L\|. \end{aligned} \tag{89}$$

Define

$$\begin{aligned} J_k \ \stackrel{\text{def}}{=}\ & \int_{C\cap D_{i_1}\neq\emptyset,\cdots,C\cap D_{i_k}\neq\emptyset} \|C_j \cap_{m=i_1,\cdots,i_k} D_m\| dD_{i_1}\ \cdots\ dD_{i_k} \\ & -(1+\rho_H)^k\Pi_{m=1}^k(2\pi\rho_0\|D_{i_m}\|)\|C_j \cap \Omega_H\| \\ & -(1-\rho_L)^k\Pi_{m=1}^k(2\pi\rho_0\|D_{i_m}\|)\|C_j \cap \Omega_L\|. \end{aligned}$$

Then, the equation above can be described as $J_k \approx 2\pi\rho_0\|D_{i_k}\|J_{k-1}$. Therefore, $J_k \approx (2\pi\rho_0)^k\Pi_{j=1}^k\|D_{i_j}\|J_0 = (2\pi\rho_0)^k\Pi_{j=1}^k\|D_{i_j}\|(\|C_j\| - \|C_j \cap \Omega_H\| - \|C_j \cap \Omega_L\|)$.

$$\begin{aligned} & \int_{\{C\cap D_i\neq\emptyset\}_{i=1}^l} \|C_j \cap_{m=i_1,\cdots,i_k} D_m\| dD_{i_1}\ \cdots\ dD_{i_k} \\ =\ & g_2(C_j,k)\Pi_{i=i_1,\cdots,i_k}(2\pi\rho_0\|D_i\|) \end{aligned} \tag{90}$$

By applying this result to Eq. (84), we obtain Eq. (27).